Volume 1 | Number 1 | Jan 2013 | Pages 1–100

Dalton Transactions

An international journal of inorganic chemistry
www.rsc.org/dalton

ROYAL SOCIETY OF CHEMISTRY

ROYAL SOCIETY OF CHEMISTRY

www.rsc.org/dalton

The two different porphyrin-chromophores, the dyad **(PorZn)$_2$-NMe$_2$** and the triad **PorZn-(PorCOOH)$_2$-(piper)$_2$** have been synthesized and their photophysical and electrochemical properties have been investigated: they also has been tested as DSSC.
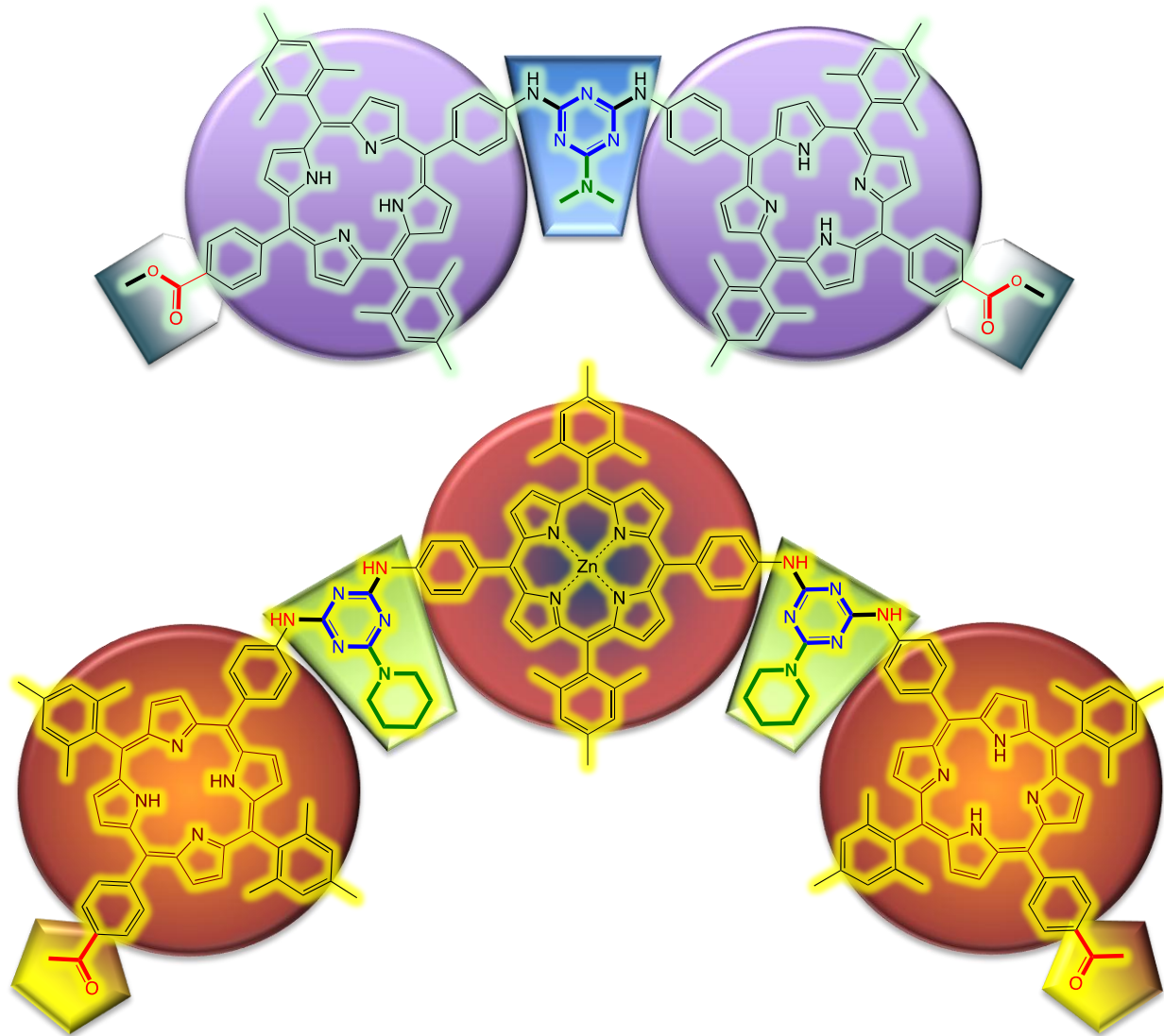
Triazine di(carboxy)Porphyrin Dyad versus a Triazine di(carboxy) Porphyrin Triad for sensitizers in DSSC

G. E. Zervaki,[1] Vasilitsa Tsaka,[1]Alexandra Vatikioti,[1] Irene Georgakaki, [1] Vasilis Nikolaou,[1] G. D. Sharma,[2*]A. G. Coutsolelos[1*]

[1]Department of Chemistry, Laboratory of Bioinorganic Chemistry, University of Crete, Voutes Campus, P.O. Box 2208, 71003

Heraklion, Crete, Greece

[2]R&D Centre for Engineering and Science, JEC Group of Colleges, Jaipur Engineering College Campus, Kukas, Jaipur, Raj 303101, India

Abstract

Two porphyrin-chromophores, i.e. the **triad PorZn-(PorCOOH)$_2$-(piper)$_2$ (GZ-T1)** and the dyad **(PorZn)$_2$-NMe$_2$ (GZ-D1)** have been synthesized and their photophysical and electrochemical properties have been investigated. The optical properties together with the appropriate electronic energy levels, i.e. the highest occupied molecular orbital (HOMO) and the lowest unoccupied molecular orbital (LUMO) energy levels revealed that both porphyrin assemblies can function as sensitizers for dye sensitized solar cells (DSSCs). The **GZ-T1** and **GZ-D1**-based DSSCs have been prepared and studied using 20 mM CDCA as coadsorbent and found to exhibit an overall power conversion efficiency (PCE) of 5.88 % and 4.56 %, respectively (under illumination intensity of 100 mW/cm^2 with TiO$_2$ films of 12μm). The higher PCE of the **GZ-T1**-sensitized DSSC, as revealed from the current-voltage characteristic under illumination and the incident photon to current conversion efficiency (IPCE) spectra of the two DSSCs, is mainly attributed to its enhanced short circuit current (J$_{sc}$), although both the open circuit voltage (V$_{oc}$) and the fill factor are improved too. The electrochemical impedance spectra (EIS) demonstrated shorter electron transport time, longer electron lifetime and higher charge recombination resistance for the DSSC sensitized with dye **GZ-T1** as well as larger dye loading onto the TiO$_2$ surface.

INTRODUCTION

Nowadays that the energy demand increases worldwide and the fossil fuels reserves wear out, research has been redirected towards renewable energy sources in the aim of sustainable progress and development. Along these lines, dye sensitized solar cells (DSSCs), first reported by Grätzel in 1991,[1] have been at the focus of these efforts of improving the photovoltaic technology, due to their potential direct application as they are of low cost, easy fabrication and high power conversion efficiency.[2] A typical DSSC consists of a dye sensitized photoanode (generally TiO_2) and a platinum (Pt) counter electrode sandwiching an electrolyte that contains a redox mediator. Upon absorption of light, an electron is injected from the photoexcited dye into the TiO_2 conduction band (CB). While the injected electrons move through the external circuit to the counter electrode, the oxidized dye is reduced by the redox shuttle, which is an iodine (I^-) ion or a Co^{2+} complex in the electrolyte (dye regeneration). Finally, the I^- ion or the Co^{2+} complex is regenerated by the reduction of the corresponding I_3^- ion or Co^{3+} complex at the surface of the counter electrode completing in that way the circuit. A key component of these devices is the sensitizing dye which is responsible for solar energy capturing and its subsequent conversion into electrical energy. Ruthenium-dyes, such as N3 and N719, have been reported with PCEs that surpass 11%,[3] but their widespread applications are hampered due to the high cost and difficult synthesis of ruthenium complexes. In the view of the above limitation of ruthenium based sensitizers, efficient metal free organic dyes[4] have been explored owing their potential to low cost production and facile modulation of their structure. Furthermore, their optical and electrochemical properties, i.e. their absorption profiles as well as their highest occupied molecular orbital (HOMO) and their lowest unoccupied molecular orbital (LUMO) energy levels are such that allow them to successfully mimic the ruthenium based dyes. A number of organic dyes have been reported in DSSCs to achieve relatively high PCE values with the best one as high as 10.3 %.[4c] On the other part, researchers have attempted to utilize porphyrins as sensitizers for DSSCs due to their intense absorption bands in the visible region of solar spectrum, versatile modification of their core, and facile tuning of their electrochemical properties.[5,2a] Porphyrin sensitizers exhibit a strong absorption at the Soret region (400 - 450 nm) and at the Q bands region (500 - 700 nm). They offer the great advantage of adjusting the electronic levels of their macrocycle by simply changing the porphyrin substituents

at the *meso* and β-positions, or by changing the complexed metal, with Zn^{II} proving to be the best choice for obtaining efficient sensitizers.[6] The PCE of 12.3% has been achieved in a DSSC co-sensitized by the D-π-A porphyrin dyeYD2-o-C8 (*N,N'*-diphenyl amine acts as the donor, porphyrin macrocycle as the π spacer, and the ethynylbenzoic acid moiety serves as an acceptor), and the organic dye Y123 with cobalt-based redox electrolyte.[7] Recently, Grätzel's research group sensitized a DSSC using a modified porphyrin dye SM315. That introduces a benzothiadiazole (BTD) group between the porphyrin ring and the anchoring acceptor, achieving a PCE value of 13%.[8]

The light harvesting ability of porphyrins in visible and NIR regions can be increased by incorporation of π-chromophores into porphyrins through conjugated bridges,[9] fused porphyrins[10] and various covalent non covalent porphyrin arrays.[11] Kim et al. designed a *meso-meso* linked porphyrin dimer which was used as for DSSCs sensitizer achieved a PCE value of 4.2 %.[12] The HOMO and LUMO of the dimer have the same energy as the corresponding porphyrin monomers and it shows much broader absorption bands, induced by exciton coupling. Segawa and coworkers reported a series of efficient *meso-meso* ethynyl-linked porphyrin oligomers as sensitizers.[13] Aiming to strengthen the push pull character of such systems, they introduced an electron donating amino moiety at the meso position of one of porphyrin units achieved a PCE value of 5.2 %.[13a] Furthermore, they reported an ethynyl-linked porphyrin triad for DSSC and achieved a PCE value of 3.2 %.[13c] Although ethynyl-linked porphyrins revealed a broad absorption extended to NIR region, the maximum IPCE values are limited up to only 40% probably due to insufficient electron injection and aggregation tendency. Enhancement of push-pull structures and a well-designed gradient of the energy levels of hetero-porphyrin arrays would need more consideration to strengthen the intermolecular CT character, leading to efficient electron injection and higher PCE value.

1,3,5-triazine moiety has been used as a linker for the synthesis of metal free organic dyes used as sensitizers for DSSCs and other photoconductive materials.[14] The structural, chemical and electronic properties of this unit allow the synthesis through simple organic reactions[15] of complex π-conjugated multi-chromophore dyes that offer improved light harvesting ability, as well as improved electron injection and transportation rates.[16] Liu et al. reported a solar cell, sensitized by a triazine-based

metal-free organic dye with a D–π–A structure that showed a PCE value of 3.63%.[17] Triazine–bridged porphyrin arrays have been also used as electron donors in bulk heterojunction (BHJ) solar cells by Luechai et al.[18] and recently by our research group.[19] Moreover, our group has recently developed a synthetic approach towards oligomeric porphyrinic derivatives with carboxylic acid anchoring groups.[20] Following this approach, we synthesized porphyrin dyads or triads, where the porphyrin precursors were linked either through an esteric[20a] or an amide bond[20b], also either a triazine group,[20c-f] or a triazole group[20g] obtained via click-chemistry. Similarly, we reported trimeric porphyrin systems either with linear[20b] or star-type[20f] architectures. These molecular systems were used as sensitizers in DSSCs showing moderate PCE values. The first porphyrin dyads that we reported, based on a triazine scaffold, were functionalized with a glycine anchoring group, which resulted in PCE values of 3.61% and 4.46%.[20c] In order to investigate the effect of the anchoring groups on the solar cell efficiency, we synthesized triazine linked porphyrin dyads with two and one carboxylic acid anchoring groups, and we found that the former exhibit superior performance than the latter (5.28% vs 3.50%, respectively).[20d] Aiming to examine the effect of the number of chromophore units on the photovoltaic performance, we synthesized a propeller-shaped porphyrin triad with a carboxylic acid anchoring group on one of the porphyrin units, which showed a slightly higher PCE value of 5.56%.[20f] Furthermore, taking advantage of other chromophores, such as BODIPY (BDP), we reported a porphyrin-bis(BDP) triad which yielded a PCE value of 5.17%.[20h]

Herein, we present the synthesis and characterization of two novel porphyrin dyes i.e. PorZn-(PorCOOH)$_2$-(piper)$_2$ linear triad and (PorZn)$_2$-NMe$_2$ dyad, denoted as **GZ-T1** and **GZ-D1**, respectively, both of which are functionalized by two carboxylic acid anchoring groups. The optical absorption spectra and frontier orbital energy levels of these compounds make them promising candidates as DSSC sensitizers. The PCE values of **GZ-T1** and **GZ-D1** based DSSCs were found to be 5.88% and 4.56%, respectively, using 20 mM CDCA as coadsorbent. The current voltage (J-V) characteristics under illumination as well as the incident photon to current conversion efficiency (IPCE) spectra of DSSCs based on **GZ-T1** and **GZ-D1** reveal that the higher value of PCE for the former, as compared to the one of the latter, is attributed to the enhanced value of short circuit current (J$_{sc}$), although other parameters such as the open circuit voltage (V$_{oc}$) and the fill factor were also enhanced. Moreover, electrochemical impedance spectra of the devices also revealed that the recombination

resistance and the electron lifetime for solar cell sensitized with **GZ-T1** are higher than that of DSSC based on **GZ-D1**, leading to suppressed back electron recombination and reduced dark current, which is essential for efficient DSSCs.

EXPERIMENTAL DETAILS

Synthesis of material and characterization

General methods, materials, and techniques. All manipulations were carried out using standard Schlenk techniques under nitrogen atmosphere. 2,4,6-Trichloro-1,3,5-triazine (cyanuric chloride), diisopropylethylamine (DIPEA), dimethylamine, piperidine, $Zn(CH_3COO)_2.2H_2O$, Na_2SO_4, KOH and other chemicals and solvents were purchased from usual commercial sources and used as received, unless otherwise stated. Tetrahydrofuran (THF) was freshly distilled from Na/benzophenone. 5,15-bis(4-aminophenyl)-10,20-bis(2,4,6-trimethylphenyl)-porphyrin, $Por(NH_2)_2$, 5-(4-carbomethoxyphenyl)-15-(4-aminophenyl)-10,20-bis(2,4,6-trimethylphenyl)-porphyrin, $H_2(Por)$, and 5-(4-carboxyphenyl)-15-(4-aminophenyl)-10,20-bis(2,4,6-trimethylphenyl)-porphyrin, PorCOOH, were prepared according to literature procedures.[21,20h]

Synthesis of 5,15-bis(4-aminophenyl)-10,20-bis(2,4,6-trimethylphenyl)-porphyrin zinc (1): To a CH_2Cl_2 solution (15 mL) of $Por(NH_2)_2$ (40 mg, 0.055 mmol) a saturated solution (4 mL) of $Zn(CH_3COO)_2.2H_2O$ in MeOH (500 mg/20 mL) was added and the reaction mixture was stirred at room temperature overnight. The organic phase was washed with H_2O (3×10 mL), dried with Na_2SO_4 and the solvent was removed under reduced pressure. The crude product was purified by column chromatography (silica gel, CH_2Cl_2/EtOH 1%) resulting in 38 mg of a purple solid (yield: 87%). HRMS (MALDI-TOF): m/z calcd for $C_{50}H_{42}N_6Zn$, 790.2762 $[M]^+$: found 790.2760. Anal. Calcd for $C_{50}H_{42}N_6Zn$: C, 75.80; H, 5.34; N, 10.61. Found: C, 75.86; H, 5.49; N, 10.64.

Synthesis of linear triad PorZn-(PorCOOH)₂-(piper)₂ (GZ-T1): To a THF solution (2 mL) of cyanuric chloride (0.0098 g, 0.053 mmol) and DIPEA (11 μL, 0.064 mmol) a THF solution (2 mL) of porphyrin **1**, $Zn[Por(NH_2)_2]$, (0.021 g, 0.027 mmol) was added, under N_2 at 0°C. The mixture was stirred at 0°C for 15 min, and upon reaction completion (monitored by TLC), it was left to warm at room temperature. Next, a THF solution (4 mL) of porphyrin PorCOOH (0.080 g, 0.106

mmol) and DIPEA (22 μL, 0.128 mmol) were added and the mixture was stirred at room temperature overnight. Then, an excess of piperidine (104 μL, 1.06 mmol) and DIPEA (230 μL, 1.32 mmol) were added and the mixture was stirred at 65°C for 24h. The volatiles were removed under reduced pressure and after dilution in CH$_2$Cl$_2$; the residue was purified by column chromatography (silica gel, CH$_2$Cl$_2$/EtOH 4%). The desired triad **GZ-T1** was isolated as a purple solid. Yield: 0.025 g (36.6%). ^{1}H NMR (300 MHz, DMSO-d$_6$): δ_H(ppm) 11.34 (*s*, 1H), 10.95 (*s*, 1H), 9.74 (*s br*, 4H), 8.85 (*m*, 10H), 8.61 (*s br*, 10H), 8.32 (*s br*, 16H), 8.03 (*m*, 12H), 7.27 (*s br*, 12H), 3.37 (*s br*, 16H), 3.22 (*s*, 4H), 1.70 (*s br*, 36H), 1.19 (*s*, 18H), -2.74 (*s*, 4H). HRMS (MALDI-TOF): *m/z* calcd for C$_{168}$H$_{145}$N$_{24}$O$_4$Zn, 2626.1094 [M+H]$^+$: found 2626.1127. UV-vis (CHCl$_3$), λ / nm ($\varepsilon \times 10^{-3}$/ M^{-1} cm^{-1}): 423 (991.0), 516 (33.2), 551 (41.6), 591 (15.9), 648 (8.4). Anal. Calcd for C$_{168}$H$_{144}$N$_{24}$O$_4$Zn: C, 76.77; H, 5.52; N, 12.79. Found: C, 76.51; H, 5.59; N, 12.64.

Synthesis of dyad (PorZn)$_2$-NMe$_2$ (GZ-D1): To a THF solution (2 mL) of cyanuric chloride (0.0095 g, 0.052 mmol) and DIPEA (11 μL, 0.062 mmol) a THF solution (2 mL) of porphyrin H$_2$(Por) (0.040 g, 0.052 mmol) was added, under N$_2$ at 0°C. The mixture was stirred at 0°C for 15 min, and upon reaction completion (monitored by TLC), it was left to warm at room temperature. Next, another solution of porphyrin H$_2$(Por) (0.080 g, 0.104 mmol) in THF (4 mL) and DIPEA (22 μL, 0.124 mmol) were added and the mixture was stirred at room temperature overnight. Finally, an excess of dimethylamine (69 μL, 1.04 mmol) and DIPEA (226 μL, 1.30 mmol) were added and the mixture was stirred at 65°C for 24h. The volatiles were removed under reduced pressure and after dilution in a solvent mixture of CH$_2$Cl$_2$/Hex in a ratio of 6:4, the residue was purified by column chromatography (silica gel, CH$_2$Cl$_2$). The desired product **4** was isolated as a purple solid. Yield: 0.060 g (69%). ^{1}H NMR (300 MHz, CDCl$_3$): δ_H(ppm) 8.94 (*d*, *J* = 4.8 Hz, 4H), 8.73 (*m*, 12H), 8.44 (*d*, *J* = 8.1 Hz, 4H), 8.32 (*d*, *J* = 8.1 Hz, 4H), 8.24 (*d*, *J* = 8.7 Hz, 4H), 8.14 (*d*, *J* = 8.7 Hz, 4H), 7.29 (*s*, 8H), 4.12 (*s*, 6H), 3.78 (*s*, 1H), 3.39 (*s*, 6H), 2.63 (*s*, 12H), 1.85 (*s*, 24H), -2.58 (*s*, 4H). ^{13}C NMR (75 MHz, CDCl$_3$): δ_C 167.5, 147.1, 139.5, 139.2, 138.5, 137.9, 136.4, 135.2, 134.7, 132.0, 131.8, 131.5, 131.1, 131.0, 130.9, 130.5, 130.4, 129.6, 128.0, 127.9, 119.8, 118.7, 118.1, 117.8, 116.5, 52.6, 36.9, 21.8, 21.6. HRMS (MALDI-TOF): *m/z* calcd for C$_{109}$H$_{95}$N$_{14}$O$_4$, 1663.7582 [M+H]$^+$: found 1663.7616. UV-vis (CH$_2$Cl$_2$), λ / nm ($\varepsilon \times 10^{-3}$/ M^{-1} cm^{-1}): 421 (685.0), 516 (45.2), 552 (18.0), 592 (10.4),

649 (11.1). Anal. Calcd for $C_{109}H_{94}N_{14}O_4$: C, 78.68; H, 5.69; N, 11.78. Found: C, 78.56; H, 5.59; N, 11.85.

Metallation and ester hydrolysis. To a CH_2Cl_2 solution (15 mL) of **4** (50 mg, 0.030 mmol) a saturated solution (5 mL) of $Zn(CH_3COO)_2.2H_2O$ in MeOH (500 mg/20 mL) was added and the reaction mixture was stirred at room temperature overnight. The organic phase was washed with H_2O (3×10 mL), dried with Na_2SO_4 and the solvent was removed under reduced pressure. The crude product was purified by column chromatography (silica gel, CH_2Cl_2/EtOH 1%) resulting in 49 mg of a purple solid (yield: 91%). Next, this metallated product (49 mg, 0.027 mmol) was diluted in THF (36 mL), followed by the addition of 9.5 mL of MeOH, 12 mL of H_2O and KOH (0.735 g, 0.013 mol). After stirring the reaction mixture at room temperature overnight, the organic solvents were removed under reduced pressure and then a solution of HCl (0.5M) was added dropwise, until pH~6. The precipitate was filtered, washed with water, extracted with CH_2Cl_2 and purified by column chromatography (silica gel, CH_2Cl_2/EtOH 4%). The final product **GZ-D1** was isolated as a purple solid. Yield: 0.040 g (84%). ^{1}H NMR (300 MHz, CDCl$_3$/MeOD 1:0.01): δ (ppm) 8.95 (*d*, *J* = 4.8Hz, 5H), 8.75 (*m*, 11H), 8.43 (*d*, *J* = 7.8Hz, 4H), 8.31 (*d*, *J* = 8.1Hz, 4H), 8.22 (*d*, *J* = 8.4Hz, 4H), 8.10 (*d*, *J* = 8.1Hz, 4H), 6.97 (*s*, 9H), 6.55 (*s*, 2H), 3.36 (*s*, 6H), 2.61 (*s*, 12H), 1.82 (*s*, 24H); HRMS (MALDI-TOF): *m/z* calcd. for $C_{107}H_{89}N_{14}O_4Zn_2$: 1761,5539 [M+3H]$^+$, found 1761.5542. UV-vis (THF), λ/nm ($\varepsilon \times 10^{-3}$/M^{-1} cm^{-1}): 426 (300.0), 558 (14.4), 599 (5.5). Anal. Calcd for $C_{107}H_{86}N_{14}O_4Zn_2$: C, 72.91; H, 4.92; N, 11.12. Found: C, 72.83; H, 4.97; N, 11.29.

NMR spectra. ^{1}H NMR and ^{13}C NMR spectra were recorded on a Bruker DPX-300 MHz spectrometer, as solutions in deuterated solvents by using the solvent peak as the internal standard.

Mass spectra. High-resolution mass spectra were recorded on a Bruker UltrafleXtreme MALDI-TOF/TOF spectrometer.

FTIR spectra. FTIR were recorded on a Perkin Elmer 16PC FTIR spectrometer.

Photophysical measurements. UV-vis absorption spectra were measured on a Shimadzu UV-1700 spectrophotometer using 10 mm path-length cuvettes. Emission spectra were measured on a JASCO FP-6500 fluorescence spectrophotometer

equipped with a red sensitive WRE-343 photomultiplier tube (wavelength range: 200-850 nm).

Electrochemistry measurements: Cyclic and square wave voltammetry experiments were carried out at room temperature using an AutoLab PGSTAT20 potentiostat and appropriate routines available in the operating software (GPES, version 4.9). Measurements were carried out in freshly distilled and deoxygenated CH_2Cl_2, with scan rate 100 mV/s, with a solute concentration of 1.0 mM in the presence of tetrabutylammoniumhexafluorophosphate (0.1 M) as supporting electrolyte. A three-electrode cell setup was used with a platinum working electrode, a saturated calomel (SCE) reference electrode, and a platinum wire as counter electrode. The system was calibrated by ferrocene.

Computational details: Theoretical calculations (DFT,[22] TDDFT,[23]) were performed at the B3LYP/6-31G(d)[24,25] level of theory using Gaussian 03 program suite.[26] TDDFT calculations were carried out using geometry optimized coordinates in same level of theory and basis sets. The computed structures and molecular orbitals were modeled using ChemCraft software.[27]

Fabrication and characterization of DSSCs.

A detailed description of the preparation of the DSSCs was reported elsewhere by our research group.[20] The J−V characteristics of the DSSCs were measured using a computer-controlled Keithley source meter, under standard air mass (AM 1.5, 100 mW/cm^2), using a xenon lamp coupled with an optical filter. The IPCE spectra of the DSSCs were recorded using a system consisting of a monochromator and a xenon lamp, and the photocurrent in short-circuit conditions was measured using a Keithley electrometer. The EIS measurements of DSSCs, in the dark as well under illumination, were carried out by applying a bias equivalent to the open circuit voltage, recording over a frequency of 0.1−100kHz with an alternating-current amplitude of 10 mV. The above measurements were carried out using a CHN electrochemical workstation equipped with FRA software to analyze the data.

RESULTS AND DISCUSSION

Synthesis. As shown in Scheme 1, the porphyrin triad PorZn-(PorCOOH)$_2$-(piper)$_2$ **(GZ-T1)**, consists of a *meso* aryl-substituted zinc metallatedporphyrin unit,

Zn[Por(NH$_2$)$_2$], (namely 5,15-bis(4-aminophenyl)-10,20-bis(2,4,6-trimethylphenyl) porphyrin) zinc, which is connected, through its aryl-amino groups at its periphery, with two other *meso* aryl-substituted free-baseporphyrin units, abbreviated as PorCOOH, (namely 5-(4-carboxyphenyl)-15-(4-aminophenyl)-10,20-bis(2,4,6-trimethylphenyl)porphyrin), by using two 1,3,5-triazine moieties as bridges. Each of the peripheral free-baseporphyrin units contains, also, a carboxylic acid as an anchoring group, for attachment onto the TiO$_2$ surface of DSSC electrodes. On the other hand, the porphyrin dyad (PorZn)$_2$-NMe$_2$ **(GZ-D1)** contains two *meso*-substituted zinc metallated porphyrin moieties, connected to each other through their aryl-amino groups at their peripheries by a 1,3,5-triazine moiety. Each of the porphyrin moieties bears an anchoring carboxyl group. In addition, the 1,3,5-triazine moiety is covalently attached to a dimethylamine group, making the whole compound to have a "push - pull" structure.[28] This property is based on a "donor–π–acceptor" (D–π–A) architecture, where π is considered to be the π-conjugated porphyrin unit connected to the triazine moiety, D represents the dimethylamine group and A is the carboxylic acid anchoring group.

The syntheses of the triad and the dyad, shown in Scheme 2 and Scheme 3, respectively, were accomplished via stepwise amination reactions of cyanuric chloride, which is the precursor of the bridging 1,3,5-triazine group of the triad. The cyanuric chloride in known to provide access to a variety of triazine-bridged assemblies, such as macrocycles,[29] dendrimers,[30] and multiporphyrin arrays.[31,32] Furthermore, we have recently reported symmetrical and unsymmetrical triazine-bridged porphyrin dyads and triads.[19,20]

The initial step for the synthesis of the triad PorZn-(PorCOOH)$_2$-(piper)$_2$ **(GZ-T1)** involves, after the zinc metallation of Por(NH$_2$)$_2$, the reaction of one equivalent of Zn[Por(NH$_2$)$_2$] **(1)** with two equivalents of cyanuric chloride, in the presence of the base DIPEA at 0°C in THF (Scheme 2). TLC indicating the disappearance of the reactants monitored the reaction and the formation of the porphyrin adduct **1a**. The latter was not isolated but further reacted at room temperature with PorCOOH moiety, followed by the substitution of the third chlorine atom of cyanuric chloride by an excess of piperidine, in an one-pot reaction at 65°C. As a result, the desired PorZn-(PorCOOH)$_2$-(piper)$_2$ triad **(GZ-T1)** was produced, as confirmed by ^{1}H NMR spectroscopy and MALDI-TOF spectrometry. It is worth mentioning that in the ^{1}H

NMR spectrum of PorZn-(PorCOOH)$_2$-(piper)$_2$ **(GZ-T1),** the signals of the aromatic hydrogen atoms of the *ortho* position to the amino groups of PorCOOH moiety, after attachment to the triazine ring, are shifted downfield compared to those of free PorCOOH.

The synthesis of the dyad (PorZn)$_2$-NMe$_2$ **(GZ-D1)** follows a similar manner. Firstly, one equivalent of cyanuric chloride was reacted with one equivalent of H$_2$(Por), in the presence of the base DIPEA at 0°C in THF (Scheme 3). The reaction was monitored by TLC and upon   disappearance of the reactants, an excess of H$_2$(Por) was added, at room temperature, producing the porphyrin adduct **3**. The substitution of the third chlorine atom of cyanuric chloride by an excess of dimethylamine, in an one-pot reaction at 65°C, resulted in the formation of the precursor porphyrin dyad **(4)**, as confirmed by ^{1}H and ^{13}C NMR spectroscopy and MALDI-TOF spectrometry. Next, zinc metallation of the porphyrin units of **4** and basic hydrolysis of the ester groups in their peripheries produced the desired final (PorZn)$_2$-NMe$_2$ dyad **(GZ-D1)**, as confirmed by ^{1}H NMR spectroscopy and MALDI-TOF spectrometry.

Photophysical properties. The optical absorption spectra of **GZ-T1** and **GZ-D1** in THF solution are shown in Figure 1(a) and 1(b) (black lines). Both **GZ-T1** and **GZ-D1** show the characteristics absorption bands of porphyrins, i.e. an intense Soret band in 420- 440 nm range and moderate Q bands between 500 nm to 680 nm. The absorption spectra of both porphyrins adsorbed onto TiO$_2$ films were also obtained (red line in Figure 1(a) and 1(b)), in order to get information about their light harvesting ability when they are used as sensitizers for dye sensitized solar cells. Compared to the corresponding solution spectra, the absorption bands of both **GZ-T1** and **GZ-D1** adsorbed on the TiO$_2$ film are broader and red-shifted due to the interactions between the porphyrins and TiO$_2$ surface. The optical band-gap of **GZ-T1** and **GZ-D1** were estimated from the absorption onset edge of the absorption spectra adsorbed onto TiO$_2$ and they are found to be about 1.82 eV and 1.92 eV, respectively. The steady state fluorescence (FL) spectra of **GZ-T1** and **GZ-D1** in THF solution are shown in Figure 2 (black and red lines, respectively). Excitation of both porphyrins at their Soret bands results in photoluminescence with two peaks of unequal intensities 609 nm and 658 nm for **GZ-D1** and three peaks (660 nm (intense), 609 nm and 716 nm (low intensity) for **GZ-T1**. A significant spectral shift was obtained for **GZ-T1** compared to **GZ-D1**, which is similar to the Q-band absorption pattern obtained in optical absorption spectra. These results indicate that the triad **GZ-T1** has increased

conjugation as compared to dyad **GZ-D1,** a feature that could differentiate their optical properties and in turn the photocurrent generated in DSSC devices.

The 0-0 transition energy E_{0-0} values were estimated for the **GZ-T1** and **GZ-D1** from the intersection of the normalized absorption and emission spectra in THF solution and they are found to be 1.94 eV and 2.04 eV, respectively. The low value of E_{0-0} for **GZ-T1** is in accordance with the increase in conjugation length.

Electronic properties. The electrochemical properties of porphyrin compounds **GZ-T1** and **GZ-D1** were investigated by cyclic voltammetry measurements, in order to conclude the feasibility of electron injection from the excited state of porphyrins into the conduction band of TiO_2 as well as their regeneration by the I_3^- / I^- redox couple in the electrolyte. The cyclic voltammograms of both porphyrin dyes in DCM are displayed in Figure 3 and electrochemical data are summarized in Table 1. Both porphyrins **GZ-T1** and **GZ-D1** exhibit the first reversible oxidation process at potential E_{ox}^1 0.67 V vs SCE and 1.03 V vs SCE, respectively and the first reversible reduction at potential E_{red}^1 -1.30 V vs SCE and -1.38 V vs SCE, respectively. In DSSCs, for efficient electron injection from the excited state of sensitizer into the CB of TiO_2, the lowest unoccupied molecular orbital (LUMO) energy level (first reduction potential observed in CV) should be higher (more negative) than the CB edge (-0.74 V vs SCE) of TiO_2. Both porphyrin compounds **GZ-T1** and **GZ-D1** show indeed E_{red}^1 values, which are more negative than the CB edge of TiO_2, suggesting that there is sufficient driving force for electron injection from their excited state into the CB of TiO_2. On the other hand, in order to ensure efficient regeneration of the sensitizer (after electron injection) in the DSSC, the highest occupied molecular orbital (HOMO) energy level (corresponds to its first oxidation potential E_{ox}^1) should be lower than the corresponding redox potential of the electrolyte redox couple employed in the DSSC, i.e. I_3^- / I^- (0.4 V vs SCE). The potentials E_{ox}^1 for both **GZ-T1** and **GZ-D1** are more positive than the corresponding electrolyte redox potential, and therefore, regeneration of the porphyrin dyes, after the electron injection, is thermodynamically feasible.[28,33]

FT-IR Spectroscopy. Concerning the binding to TiO_2, while both the porphyrin dyes contain carboxylic acid groups which are known to be very good anchoring groups to the TiO_2 surface, the triad porphyrin dye **GZ-T1** in addition

contains two piperidine binding sites that could also act as anchoring group to the TiO_2 surface through its basic sp^3 hybridized N atom. In order to get information about the binding strength of **GZ-T1** and **GZ-D1** on to the TiO_2 surface, FTIR powder spectra were recorded in pure form and adsorbed on TiO_2 films. In the FTIR spectrum of **GZ-T1** in pure form (Figure 4, black color) the absorption band at 1686 cm^{-1}, corresponds to the $\nu(COO)$ stretching vibration of carboxylic acid group,[34] and it disappears upon adsorption onto TiO_2 surface while two new bands at 1404 cm^{-1} and 1532 cm^{-1}, corresponding to $\nu_{symm}(COO^-)$ and $\nu_{asym}(COO^-)$ stretching vibrations are observed (Figure 4, red color). The FTIR spectra of pure **GZ-D1** and **GZ-D1**/TiO_2 are similar. These observations indicate that both compounds **GZ-T1** and **GZ-D1** are strongly bound to the TiO_2 surface through their carboxylic acid anchoring groups. Moreover, in the FTIR spectrum of **GZ-T1** in pure form, there are two additional absorption bands at 1634 cm^{-1} and 3310 cm^{-1} (the latter not shown in the figure), which are not observed in the FTIR spectrum of **GZ-D1**. These bands can be assigned to the $\nu(C=N)$ and $\nu(N-H)$ stretching vibrations of the piperidine rings respectively and they disappear when **GZ-T1** is adsorbed onto the TiO_2 film. This suggests that in triad **GZ-T1**, in addition to the carboxylic acid anchoring group, the piperidine ring might also be involved in the binding to the TiO_2 surface, through the nitrogen atom.

DFT Calculations. In order to further explore the molecular structures, as well as to get insight into the electron density distribution of the frontier molecular orbitals (FMOs) of the porphyrin triad PorZn-(PorCOOH)$_2$-(piper)$_2$ (**GZ-T1**) and the porphyrin dyad (PorZn)$_2$-NMe$_2$ (**GZ-D1**) DFT calculations were carried out.

The gas-phase geometry optimized structures of the two compounds are presented in Figure 5, while the corresponding coordinates are provided in Tables S1, S2 respectively (see Supporting Information). In triad **GZ-T1**, three almost co-planar porphyrin units are bridged by two perpendicularly oriented triazine groups (see also Figure S1). Dyad **GZ-D1** is found to exhibit a similar structure with the central triazine group adopting a perpendicular orientation with respect to the two terminal porphyrin units (see also Figure S2). Therefore, in both cases the bridging triazine units do not allow the formation of extended π-conjugated systems, a fact that has a profound effect on the electronic communication between the porphyrin units.

The electron density maps and the corresponding energies of the FMOs of triad **GZ-T1** and dyad **GZ-D1** are depicted in the upper and lower part of Figure 6,

respectively. Regarding triad **GZ-T1**, in two of the highest-energy molecular orbitals (HOMO and HOMO-3) electron density is mainly spread over the central zinc-porphyrin unit and the partially on the bridging triazine groups. The four lowest-energy unoccupied molecular orbitals are very close in energy, while their corresponding electron densities are predominantly located on either of the two terminal free-base porphyrin units, with some additional contributions on the respective the carboxylic acid groups and bridging phenyl groups. Porphyrin triad **GZ-T1** can be described as a "push-pull" D-π-2A system, with the central zinc-porphyrin unit as donor D group, the terminal free-base porphyrin units with the carboxylic acid groups as acceptor A groups, and π denoting the triazine ring. Therefore, upon photo-excitation, intramolecular electron transfer from the zinc-porphyrin to the free-base porphyrin units and subsequent electron injection through the carboxylic acid groups into the TiO_2 conduction band are favorable.

The electronic density distributions in the frontier orbitals of **GZ-D1** revealed that LUMO orbitals are very close comparing their energy levels. The electron density of HOMO orbitals is located on the porphyrin units and on the bridging triazine unit, while the density of LUMO is located on the phenyl ring bearing the carboxylic acid. Those attributes propose that **GZ-D1** is a "push-pull" D-π-A system with each porphyrin unit acting as donor and acceptor in separate cases. In case of HOMO and HOMO-2 the one zinc porphyrin acts as donor group while the other zinc porphyrin acts as acceptor (LUMO and LUMO+2). On the contrary HOMO-1 and LUMO+1 reveal that the role of each porphyrin is inverted. Consequently, **GZ-D1** advances the electron injection and possess suitable frontier orbital energy levels for use as sensitizer in DSSCs

The calculated HOMO and LUMO energies, dipole moments and HOMO-LUMO gaps in dichloromethane as solvent medium for compounds **GZ-T1** and **GZ-D1** are presented in Table 2. The HOMO-LUMO gaps of both compounds are found to be similar to the corresponding values obtained from electrochemistry measurements presented in Table 1.

TD-DFT calculations at the B3LYP/6-31G(d) level using the calculated geometry-optimized coordinates of the compounds **GZ-T1** and **GZ-D1** were carried out in order to extract their theoretical UV-Vis absorption spectra (Figures S3, S4 in Supporting Information) and the electronic transitions with the molecular orbital composition (Table 3). The results for triad **GZ-T1** revealed intense peaks on 549.7

nm, 545.0 nm and 543.2 nm with oscillator strengths 0.1739, 0.0889 and 0.0853, respectively. The contributions referred to the above peaks involve transitions mainly from HOMO-3$\rightarrow$LUMO+4, HOMO$\rightarrow$LUMO+5, HOMO-1$\rightarrow$LUMO+1 and HOMO-2$\rightarrow$LUMO+2 (Table 3). These can be assigned to porphyrin-based π–π* transitions and correspond to the porphyrin Q-bands. Two more intense peaks are found at higher wavenumbers, namely at 580.6 nm and 578.9 nm with oscillator strengths 0.0742 and 0.607 respectively, which implicate contributions from HOMO-1$\rightarrow$LUMO+1, HOMO-1$\rightarrow$LUMO+3, HOMO-2$\rightarrow$LUMO+1 and HOMO-2$\rightarrow$LUMO+3 transitions. One more high intensity peak appears at 453.3 nm with 0.0217 oscillator strength, which mainly involves contribution from HOMO-1$\rightarrow$LUMO+4 transition and corresponds to the porphyrin Soret band. In case of the theoretically calculated UV-Vis spectrum of dyad **GZ-D1** (Figure S4), intense absorption peaks are found in the region 390 nm to 425 nm, which correspond to the Soret band of the porphyrin units. The oscillator strengths and the contribution of the FMOs for these peaks are listed in Table 3. One more peak at 549.5 nm with 0.126 oscillator strength is observed, which mainly involves contribution from the HOMO$\rightarrow$LUMO+1 transition and corresponds to the porphyrin Q-band.

Photovoltaic properties

The current –voltage (J-V) characteristics under illumination of the DSSCs based on **GZ-T1** and **GZ-D1** porphyrin dyes, in identical conditions are shown in Figure 7(a) and the corresponding photovoltaic parameters are summarized in Table 4. The DSSC sensitized with **GZ-T1** exhibits J_{sc} = 12.18 mA/cm^2, V_{oc} = 0.68 V and FF = 0.71, resulting in an overall PCE value of 5.88 %, whereas, DSSC based on **GZ-D1** sensitizer displayed a lower PCE value of 4.56 % with J_{sc} = 10.32 mA/cm^2, V_{oc} = 0.65 V and FF = 0.68. The higher value of PCE for the solar cell sensitized with **GZ-T1** porphyrin dye is mainly attributed to the enhanced value of J_{sc}, although other photovoltaic parameters, i.e. V_{oc} and FF are also slightly improved as compared to DSSC sensitized with porphyrin dye **GZ-D1**. The higher value for DSSC based on triad **GZ-T1** is consistent with its larger IPCE values as shown in Figure 7(b). The IPCE spectra of both DSSCs closely resemble the corresponding absorption spectra of the porphyrins adsorbed onto the TiO$_2$ film. The fact that the IPCE values in the Q-band regions are similar to the Soret band, is attributed to the scattering by the TiO$_2$

nanoparticles that increases the photocurrent in the relatively weak absorption region.[35]

The higher J_{sc} value for the DSSC based on triad **GZ-T1** is consistent with its larger values of IPCE as well as the broader profile as compared to DSSC based on dyad **GZ-D1** (Figure 7b). The IPCE is expressed as

$$IPCE = LHE \times x\eta_{inj} \times \eta_{cc}$$

where *LHE* is the light harvesting efficiency which depends on the absorption strength of sensitizer, η_{inj} is the electron injection efficiency which depends on the electron injection rate from the sensitizer into the conduction band of TiO_2 after the photoexcitation of the sensitizer, η_{cc} is the charge collection efficiency which depends on the competition between the transportation of electrons towards the external circuit and the recombination of the electrons in TiO_2 with the redox couple in the electrolyte. Among these three factors, LHE plays a key role in the efficiency of the DSSCs and it is expressed as LHE = $(1-10^{-\varepsilon\Gamma})$, where ε is molar extinction coefficient of the dye and Γ is the molar concentration of the dye loaded per surface area of the TiO_2 film. It can be seen in Figure 8 that DSSC based on **GZ-T1** exhibits a higher LHE value than **GZ-D1** based DSSC. In order to estimate the dye loading values of these DSSCs, the dye sensitized TiO_2 electrodes were immersed in a mixture of THF and NaOH (aq) solution, and the absorption spectra of these desorbed dye solutions were measured. The dye loading values were found to be 4.42 $x10^{-7}mol/cm^2$ and 3.23 $x10^{-7}mol/cm^2$, for **GZ-T1** and **GZ-D1** sensitized TiO_2 electrode, respectively. The higher dye loading for **GZ-T1** compared to **GZ-D1** may be explained by the presence of the additional piperidine binding site presented in triad **GZ-T1** which is involved in the attachment to the TiO_2 surface through nitrogen atom, as confirmed from the FTIR spectrum (vide supra).

The higher value of LHE, could lower the conduction band edge of TiO_2 upon dye uptake of the **GZ-T1** based DSSC that might lead to a larger electron injection rate to give a high electron yield for this device. This may lead to the formation of a blocking layer caused by the higher dye loading.[36]

On the basis of J-V characteristics in dark (Figure9), the DSSC based on**GZ-T1** shows a lower dark current than the **GZ-D1**-sensitized solar cell, which is directly related to the back electron recombination with the redox couple in the electrolyte. So,

the lower electron recombination rate observed in **GZ-T1** sensitized DSSC as compared to **GZ-D1**, depends mainly on the amount of dye adsorbed onto the TiO_2 surface and in turn on the degree of coverage of sensitizing dye on the surface of TiO_2. As discussed above the larger dye loading amount for the DSSC based on **GZ-T1** forms a blocking layer, which prevents charge recombination between the injected electrons in TiO_2 conduction band and I_3^- in the electrolyte. However, for porphyrin dyad **GZ-D1**, possessing a lower dye loading value, which results in lower surface coverage on the TiO_2 surface, the ions I_3^- of the electrolyte can penetrate closely to the surface of the TiO_2 decreasing the barrier for electron recombination with I_3^- resulting in a higher dark current.

The difference in the PCE value of solar cells sensitized with these two porphyrin dyes **GZ-T1** (triad) and **GZ-D1** (dyad) can also be related to their molecular structures. Considering that a Zn metallated porphyrin acts as an electron donor and a free base porphyrin unit as an electron acceptor, the triad **GZ-T1** can be considered as A-π-D-π-A and dyad **GZ-D1** as D-π-D with common anchoring carboxylic acid units, where π is denoted as the triazine π-bridge. With porphyrin dye **GZ-T1** bearing a D-π-A "push-pull" unit, a more effective electron injection in the **GZ-T1**-based DSSC is facilitated, resulting in higher value of J_{sc} and PCE.

The charge transfer and recombination processes occurring at the TiO_2/dye/electrolyte interface as important factors influencing the PCE value of the DSSC, have been analyzed by electrochemical impedance spectroscopy (EIS).[37] Figure10 shows the EIS spectra of **GZ-T1-** and **GZ-D1-**based DSSCs, in dark under a forward bias equivalent to the open circuit of the DSSC. In general, the Nyquist plots of EIS in dark showed three semicircles, in the frequency range 0.1-100 kHz. The semicircle radius in the high frequency range (left side) represents the charge transfer resistance at the counter electrode/electrolyte interface. The charge recombination at TiO_2/dye/electrolyte corresponds to semicircle in the middle frequency range. In the lowest frequency range, the impedance is associated with the Warburg diffusion processes of I_3^- in the electrolyte. As shown from the Nyquist plots of EIS (Figure10a), the radius of semicircle in the middle frequency range is larger for the DSSC based on **GZ-T1** compared to the one with **GZ-D1**, indicating large recombination resistance (R_{rec}) which in turn means slow recombination rate. The

electron lifetime (τ_e) was calculated from the peak frequency (f_{peak}) that corresponds to the middle frequency range in the Bode phase plot (Figure10b), according to the relationshipτ_e=1/2πf$_{peak}$. According to this formula, the electron lifetimes for DSSCs based on **GZ-T1** and **GZ-D1** are found to be 32 ms and 25 ms, respectively, indicating that the charge recombination is suppressed for **GZ-T1**, compared to **GZ-D1**. The higher electron lifetime for **GZ-T1** relative to **GZ-D1** could be attributed to the D-π-A nature of **GZ-T1** which disturbs the dispersion forces by trapping I_3^- near the porphyrin more effectively, preventing the approach of I_3^- towards the TiO$_2$ surface.

To get more information about the charge transport process in the DSSCs, we have also measured EIS under illumination at the bias voltage equivalent to the V$_{oc}$ of devices, and Nyquist plots for DSSCs based on **GZ-T1** and **GZ-D1** are shown in Figure 11. The semicircle in the intermediate frequency region corresponds to the charge transport process at the TiO$_2$/dye/electrolyte interface after photoexcitation. The radius of this semicircle is a measure of the charge transport resistance (R$_{ct}$) and it is smaller for the solar cell sensitized with **GZ-T1** than that for **GZ-D1**, resulting in a low value of R$_{ct}$, indicating fast transport of electrons in the TiO$_2$ film towards the FTO electrode. The electron transport time (τ_d) of an injected electron in the TiO$_2$ film is related with τ_e, τ_d, R$_{rec}$ and R$_{ct}$ as follows:

$$\frac{\tau_d}{\tau_e} = \frac{R_{ct}}{R_{rec}}$$

The electrochemical parameters i.e. R$_{rec}$, R$_{ct}$, τ_e and τ_d are summarized in Table 5. The electron transport time is a measure of the average time taken for an electron to be collected by the FTO during its transportation through the TiO$_2$ film, with a faster electron transport time associated with a higher photocurrent.[38] The decrease in R$_{ct}$ and the increase in R$_{rec}$ for the solar cell sensitized with **GZ-T1** indicate that the electron transport resistance and electron transport time decreases for the solar cell sensitized with **GZ-T1** as compared to that for **GZ-D1**.

Besides all the above parameters, the charge collection efficiency is also an important factor for achieving a high PCE value of a DSSC device. So, the charge collection efficiency of the **GZ-T1** and **GZ-D1** based DSSCs was estimated according to the relationship:[39] $\eta_{cc} = \left[1 + \left(\frac{\tau_d}{\tau_e}\right)\right]^{-1}$ and the values are found to be 0.73 and 0.54,

respectively. The higher charge collection efficiency value of **GZ-T1**-based DSSC compared to **GZ-D1**-based DSSC gives an additional explanation of its improved PCE value.

Conclusions

We have synthesized two porphyrin-based dyes, **GZ-T1** (triad) and **GZ-D1** (dyad), and investigated their optical and electrochemical (both experimental and theoretical) properties. Both of these porphyrin dyes exhibit suitable frontier orbital energy levels for efficient electron injection and dye regeneration, when used as sensitizers for DSSCs. The **GZ-T1** and **GZ-D1**-based DSSCs have been prepared using 20 mM CDCA as coadsorbent and their overall power conversion efficiency values (PCE) are measured to be 5.88 % and 4.56 %, respectively (under illumination intensity of 100 mW/cm^2 with TiO$_2$ films of 12μm). The higher PCE value for **GZ-T1** sensitized solar cell as compared to the one of **GZ-D1**, is attributed to the higher values of J$_{sc}$, V$_{oc}$ and FF, as demonstrated by the J-V characteristics, IPCE spectra and dye loading measurements. Moreover, the EIS measurements showed a longer electron lifetime and a shorter electron transport time for the DSSC based on **GZ-T1** as compared to the one with **GZ-D1**, consistent with the suppressed electron recombination which leads to higher PCE value.

Supporting Information

Cartesian coordinates, theoretically calculated UV-Vis spectrum, ^{1}H NMR and ^{13}C NMR spectra and square-wave voltammograms of **GZ-T1** and **GZ-D1**.
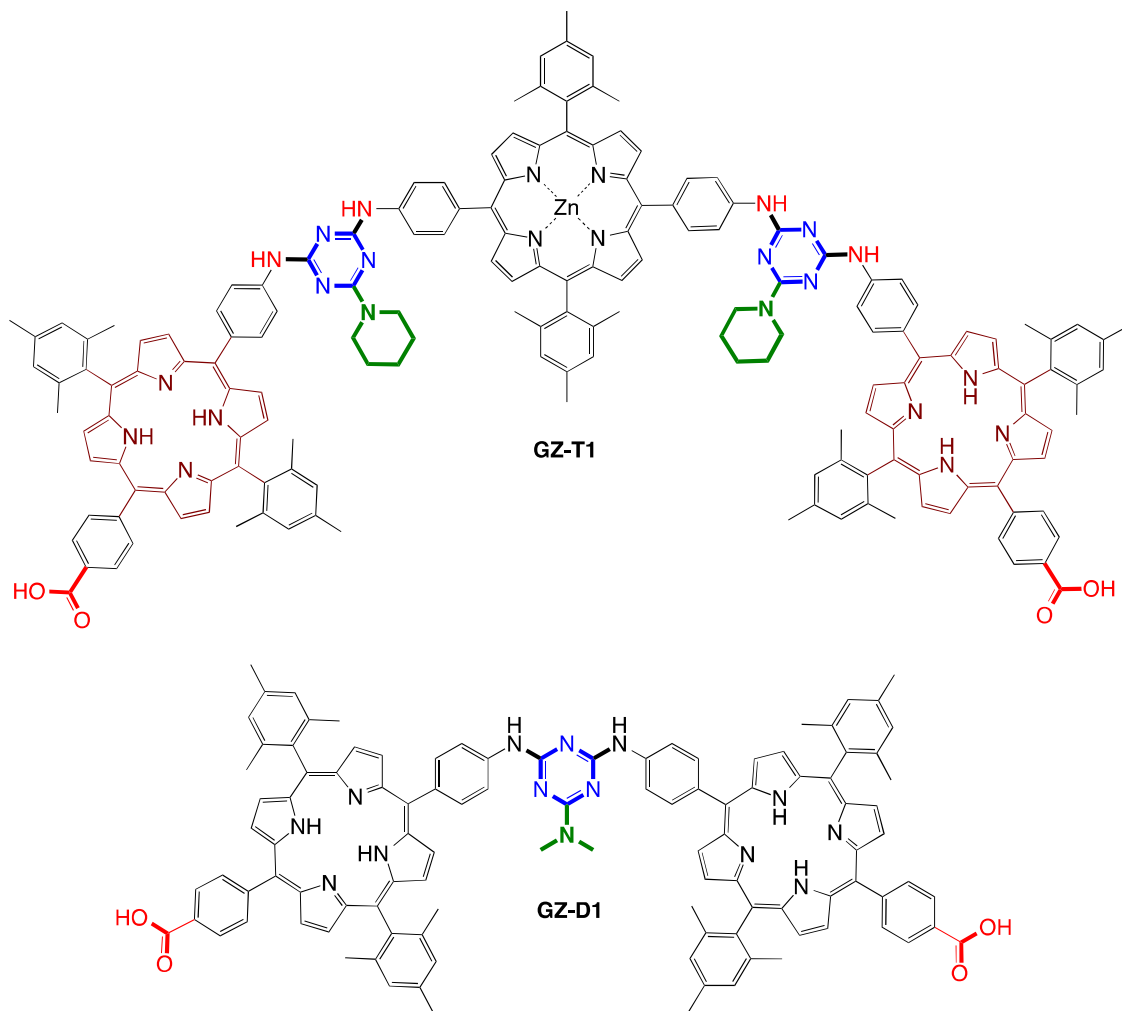
Scheme 1.   The chemical structures of the linear triad **GZ-T1** and the dyad **GZ-D1**.
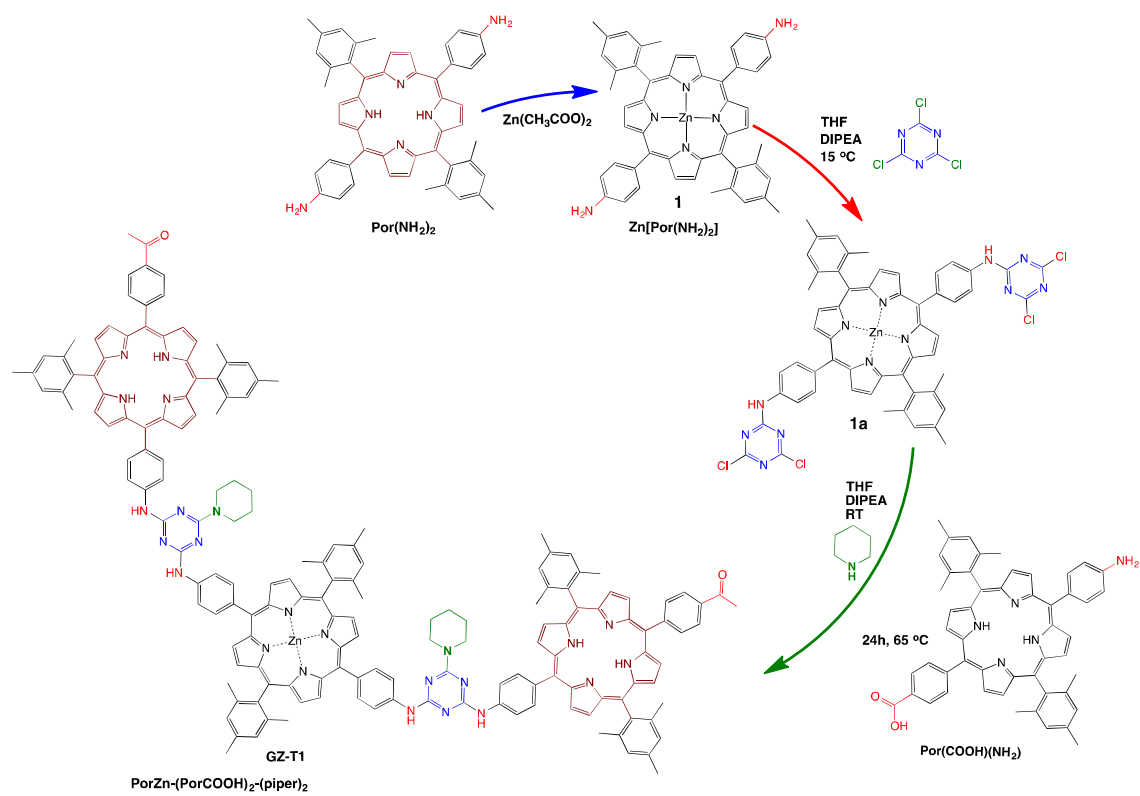
Scheme 2.   Synthesis of triad **GZ-T1**.
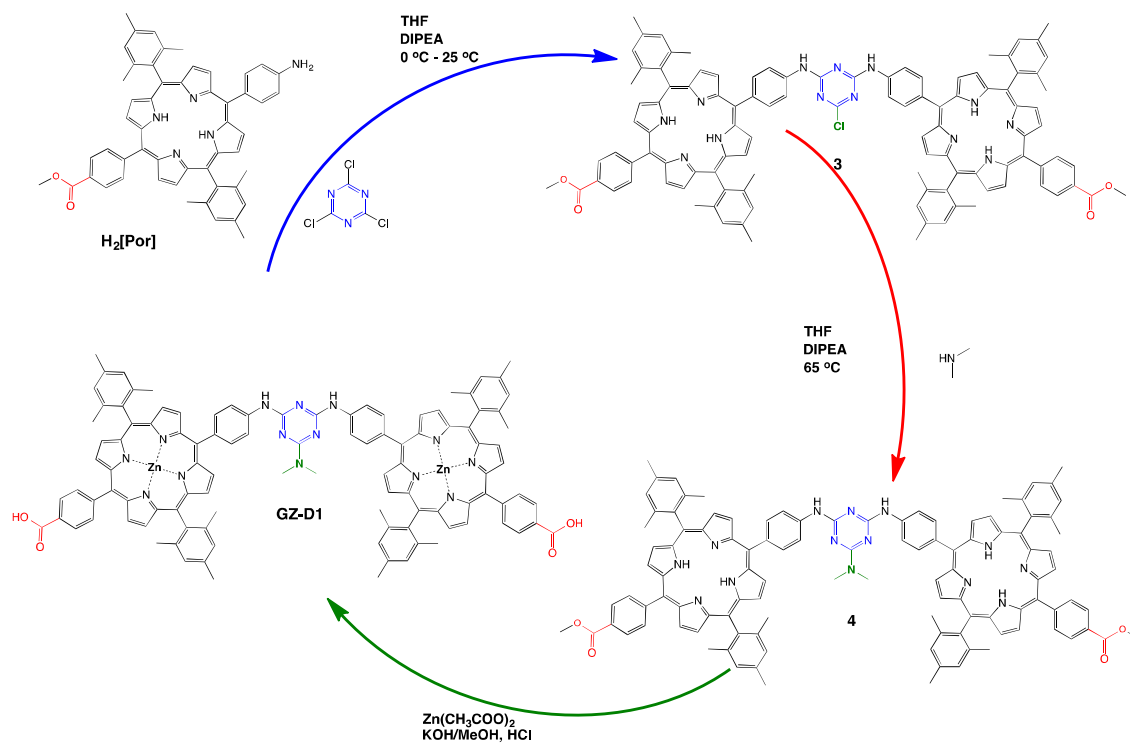
Scheme 3.   Synthesis of dyad **GZ-D1**.

Table 1 Electrochemical data and calculated band gaps E_g^{elec} for triad **GZ-T1** and dyad **GZ-D1**. The potentials are measured vs SCE.

Compound	E^1_{ox}, V	E^2_{ox}, V	E^1_{red}, V	E^2_{red}, V	E_g^{elec}, eV
GZ-T1	0.67	0.94	-1.30	-1.65	1.97
GZ-D1	1.03	1.41	-1.38	-	2.41

Table 2 DFT calculated properties of PorZn-(PorCOOH)$_2$-(piper)$_2$ **GZ-T1** and (PorZn)$_2$-NMe$_2$ **GZ-D1**: HOMO and LUMO energies, HOMO-LUMO gap and dipole moment (μ).

Compound	HOMO (eV)	LUMO (eV)	HL (eV)	μ(D)
GZ-T1	-4.973	-2.459	2.514	3.66
GZ-D1	-5.069	-2.349	2.72	4.02

Table 3   Calculated electronic transitions of PorZn-(PorCOOH)$_2$-(piper)$_2$ **GZ-T1** and (PorZn)$_2$-NMe$_2$ **GZ-D1**. The oscillator strengths, the computed wavelengths and the major orbital contributions are listed.

Compound	Theoretical (λ_{max} [nm])	Oscillator strength	Frontier orbital contribution
GZ-T1	580. 6	0.0742	HOMO-4→LUMO+1 (17.5%), HOMO-4→LUMO+3 (18.8%), HOMO-1→LUMO+1 (37.5%), HOMO-1→LUMO+3 (29.3%)
	578.9	0.0607	HOMO-5→LUMO+1 (17.0%), HOMO-5→LUMO+3 (19.9%), HOMO-2→LUMO+1 (38.5%), HOMO-2→LUMO+3 (28.0%)
	549.7	0.1739	HOMO-3→LUMO+4 (35.4%), HOMO-3→LUMO+5 (4.0%), HOMO→LUMO+4 (6.3%), HOMO→LUMO+5 (56.1%)
	545.0	0.0889	HOMO-4→LUMO+1 (20.8%), HOMO-4→LUMO+3 (14.0%), HOMO-1→LUMO+1 (28.7%), HOMO-1→LUMO+3 (32.6%)
	543.2	0.0853	HOMO-5→LUMO (21.9%), HOMO-5→LUMO+2 (13.9%), HOMO-2→LUMO (27.2%), HOMO-2→LUMO+2 (33.6%)
	453.3	0.0217	HOMO-1→LUMO+4 (92.2%), HOMO-1→LUMO+5 (6.0%)
GZ-D1	549.5	0.126	HOMO-3→LUMO+2 (3.3%), HOMO-2→LUMO+3 (34.2%), HOMO-1→LUMO (5.6%), HOMO→LUMO+1 (57.4%)
	425.0	1.551	HOMO-5→LUMO (11.3%), HOMO-4→LUMO+1 (40.5%), HOMO-3→LUMO+2 (5.9%), HOMO-2→LUMO+3 (17.3%), HOMO-1→LUMO (2.6%), HOMO→LUMO+1 (8.2%)
	418.7	0.504	HOMO-5→LUMO (41.2%), HOMO-4→LUMO+1 (7.0%), HOMO-3→LUMO+2 (15.9%), HOMO-2→LUMO+3 (4.0%), HOMO-1→LUMO (8.6%), HOMO-1→LUMO+4 (2.2%), HOMO→LUMO+1 (2.3%)
	411.3	0.357	HOMO-4→LUMO+3 (54.6%), HOMO-2→LUMO+1 (20.1%), HOMO→LUMO+3 (12.9%)
	407.8	0.543	HOMO-5→LUMO+2 (49.15%), HOMO-3→LUMO (21.7%), HOMO-1→LUMO+2 (14.5%)
	393.5	0.751	HOMO-5→LUMO (4.3%), HOMO-4→LUMO+1 (29.2%), HOMO-2→LUMO+3 (11.8%), HOMO→LUMO+5 (32.4%), HOMO-1→LUMO+4 (3.0%), HOMO→LUMO+1 (4.6%)
	385.0	0.541	HOMO-5→LUMO+2 (4.0%), HOMO-4→LUMO+3 (38.8%), HOMO-2→LUMO+1 (19.5%), HOMO-2→LUMO+5 (3.8%), HOMO→LUMO+3 (8.6%)

Table 4   Photovoltaic parameters of DSSCs based on **GZ-T1** and **GZ-D1**. CDCA (20 mM) was used as coadsorbent in each DSSC.

Porphyrin	J_{sc} (mA/cm^2)	V_{oc} (V)	FF	PCE (%)	Dye loading (mol/cm^2)
GZ-T1	12.18	0.65	0.72	5.88	4.42×10^{-7}
GZ-D1	10.32	0.68	0.68	4.56	3.23×10^{-7}

Table 5   Recombination resistance (R_{rec}), charge transport resistance (R_{ct}), electron lifetime (τ_e), charge transport lifetime (τ_d), and charge collection efficiency(η_{cc}) estimated from the EIS measurements.

Porphyrin	R_{rec} (Ω)	R_{ct} (Ω)	τ_e (ms)	τ_d (ms)	η_{cc}
GZ-T1	78	32	32	12	0.73
GZ-D1	56	44	24	18	0.57
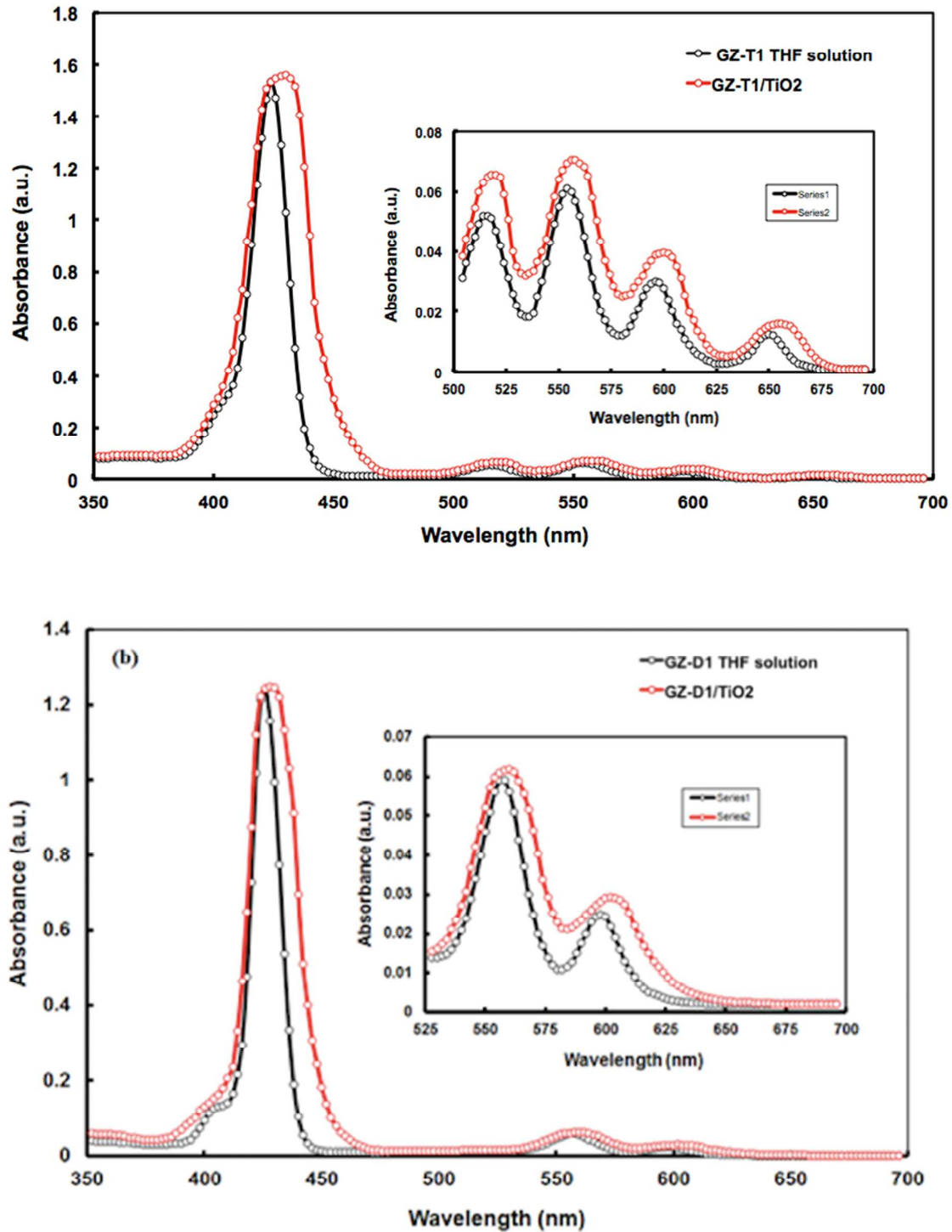
Figure 1: Normalized UV-Visible absorption spectra of (a) **GZ-T1** and (b) **GZ-D1** in THF solution (black) and adsorbed onto a TiO$_2$ film (red).
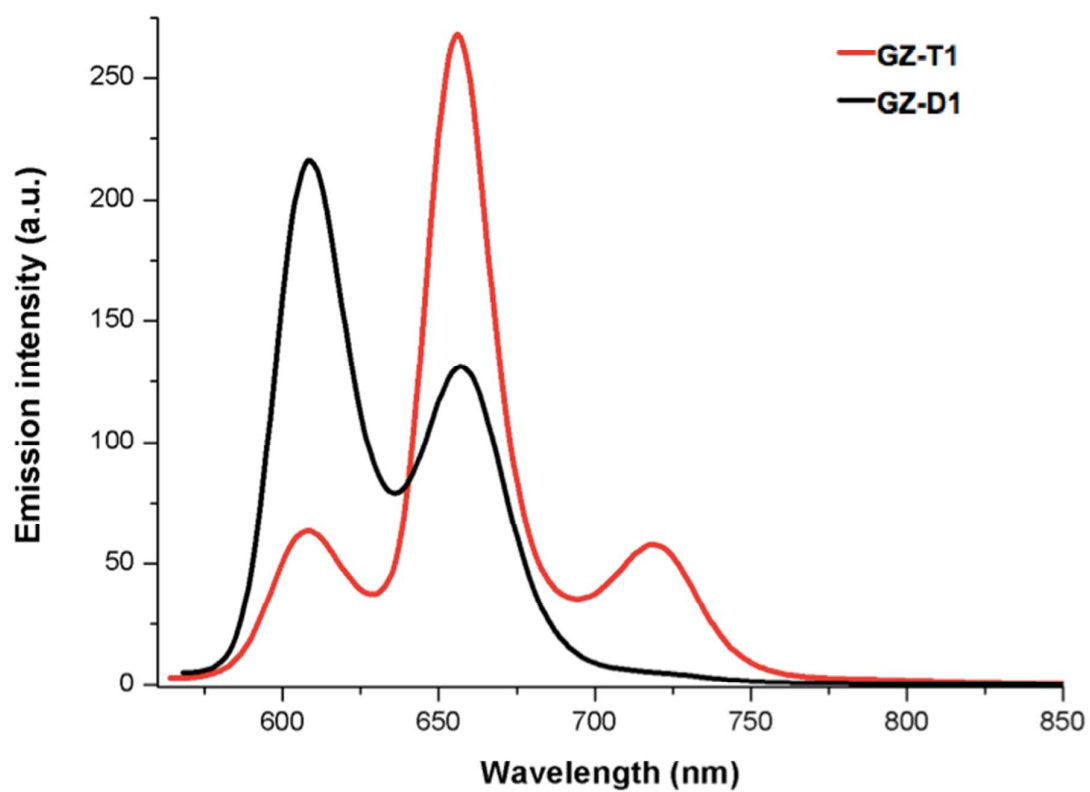
Figure 2: Isoabsorbing fluorescence spectra of **GZ-T1** (red line) and **GZ-D1** (black line) in THF.
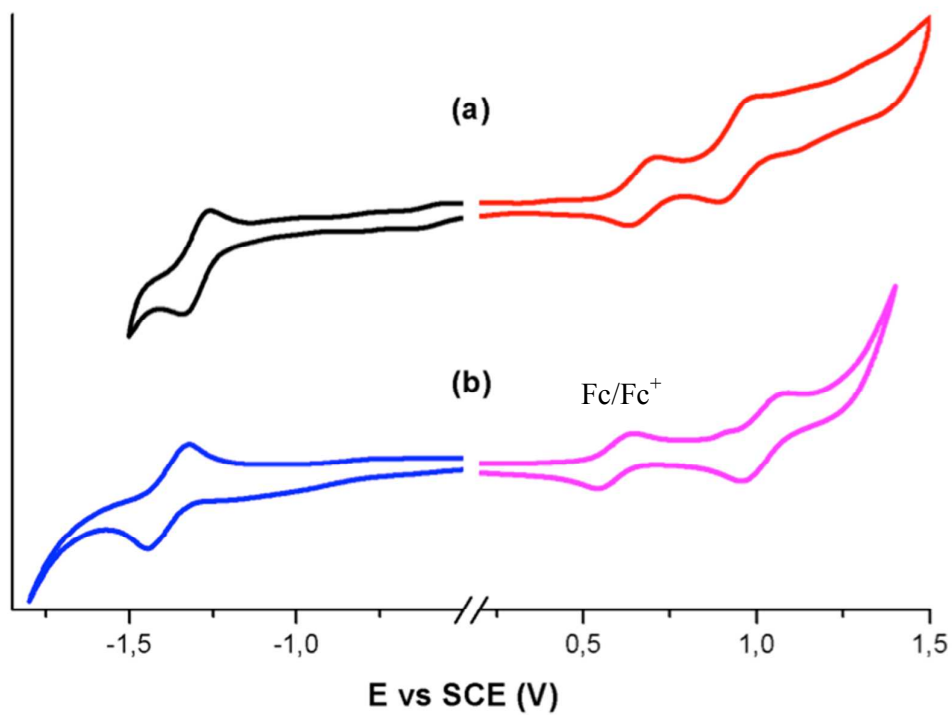
Figure 3: Cyclic voltammograms of (a) **GZ-T1** and (b) **GZ-D1** in CH_2Cl_2 solution. The ferrocene/ferrocenium ion (Fc/Fc$^+$), was found to be 0.41 V vs SCE (not shown) in voltammogram (a) and 0.59 V vs SCE in voltammogram (b).
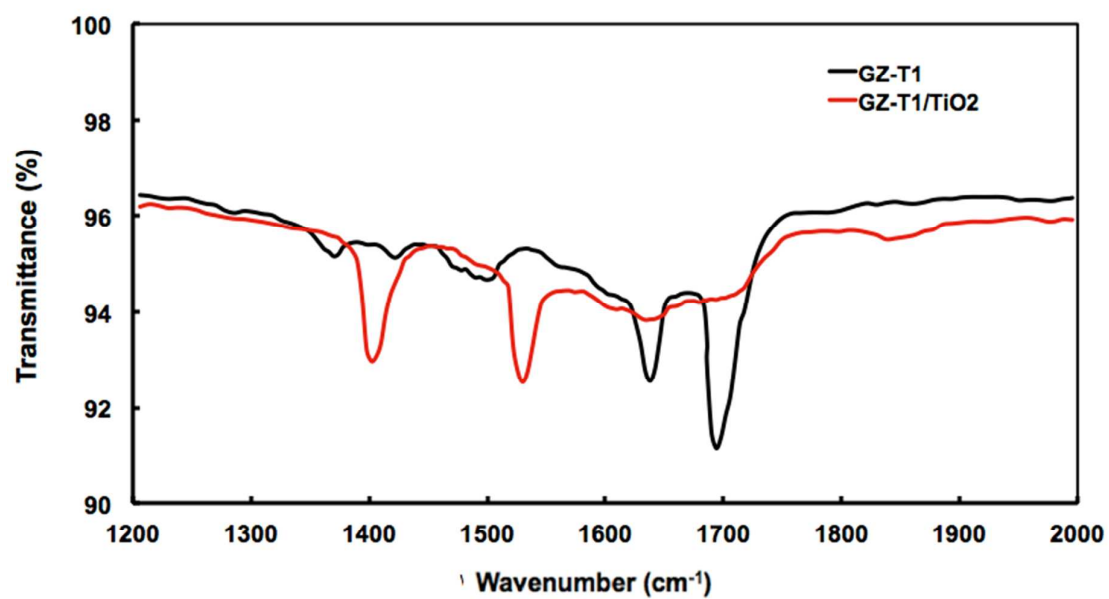
Figure 4: FTIR spectra of pristine porphyrin triad **GZ-T1** and adsorbed onto TiO$_2$.

PorZn-(porCOOH)$_2$-(piper)$_2$
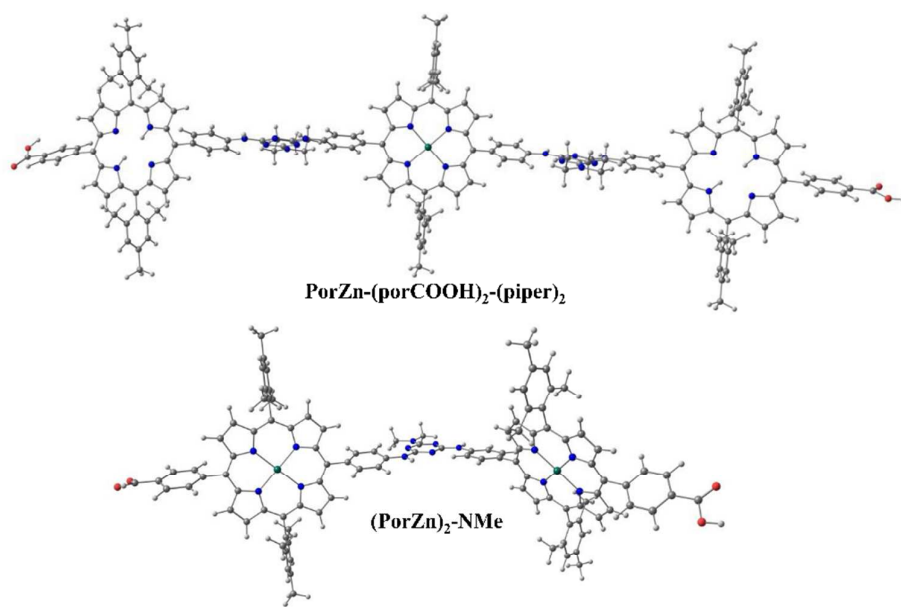
(PorZn)$_2$-NMe

Figure 5: Gas phase geometry optimized structure of PorZn-(PorCOOH)$_2$-(piper)$_2$ **GZ-T1** and (PorZn)$_2$-NMe$_2$ **GZ-D1**. Carbon, nitrogen,hydrogen, oxygen, fluoro and boron atoms correspond to grey, blue, white, red, light blue and yellow spheres, respectively.
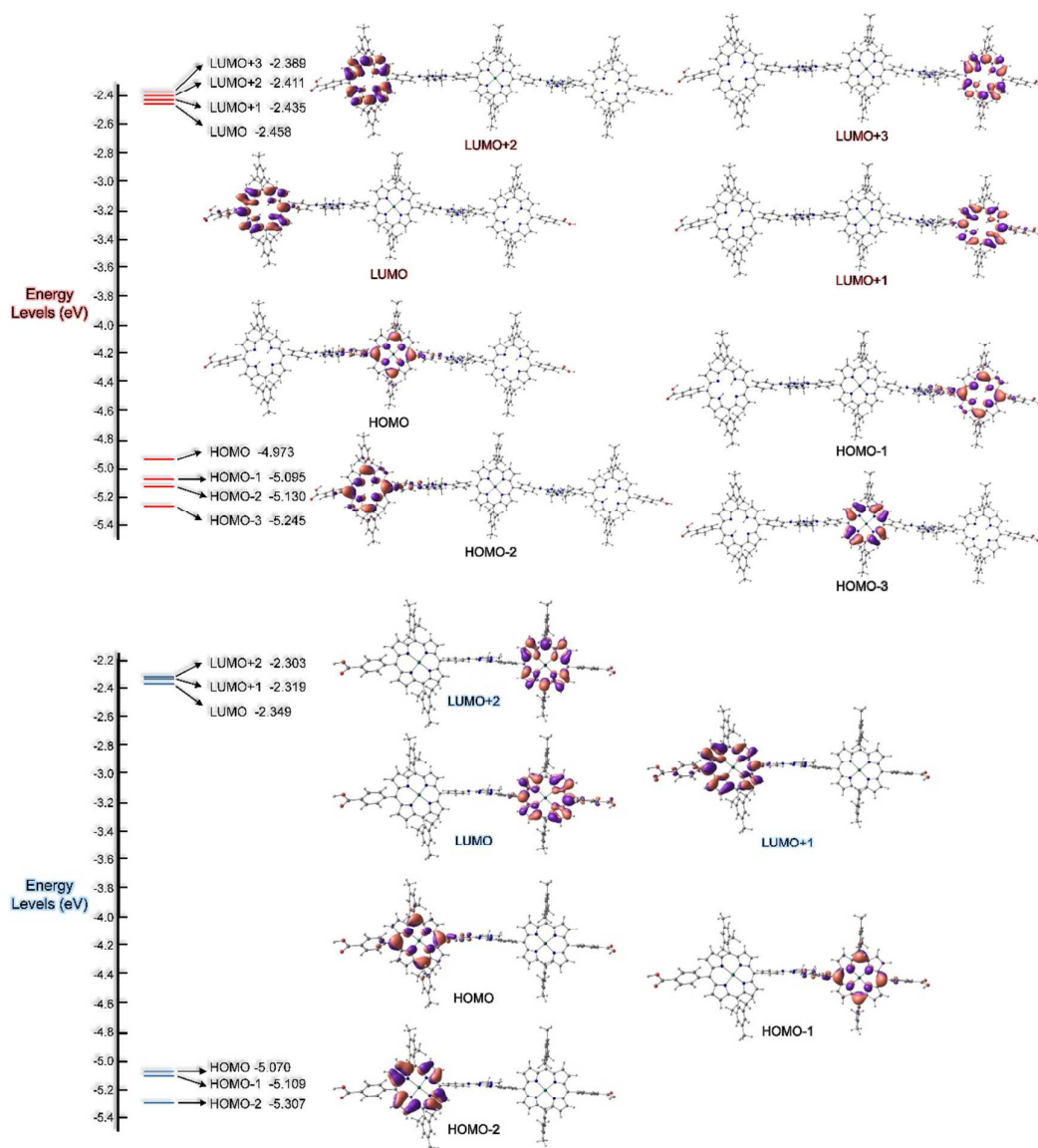
Figure 6: Frontier molecular orbitals of PorZn-(PorCOOH)$_2$-(piper)$_2$ **GZ-T1** (upper part)and (PorZn)$_2$-NMe$_2$ **GZ-D1** (lower part)   the corresponding energy levels.
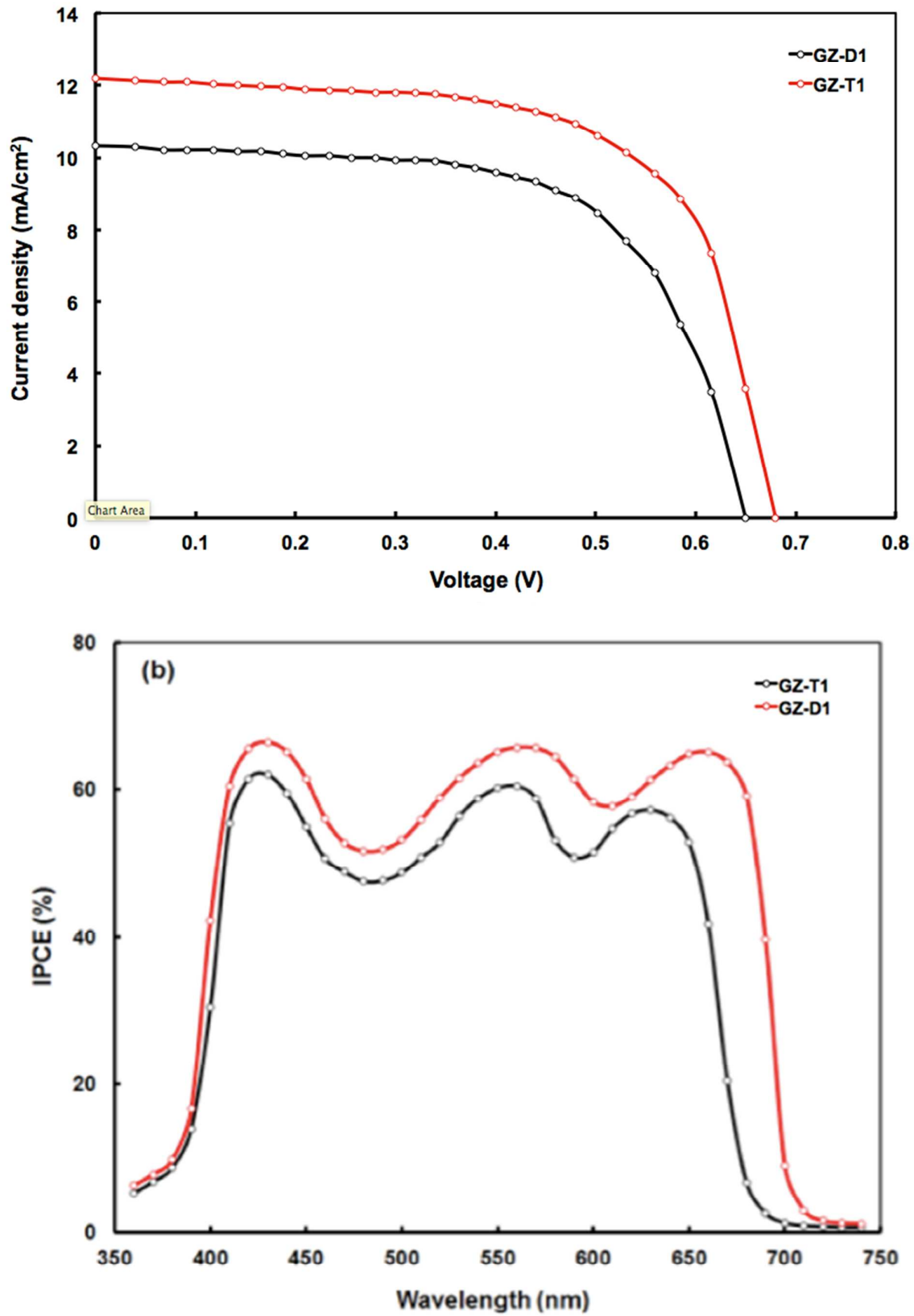
Figure 7: (a) J-V characteristics under illumination and (b) IPCE spectra of DSSCs based on porphyrin dyes **GZ-T1** and **GZ-D1**.
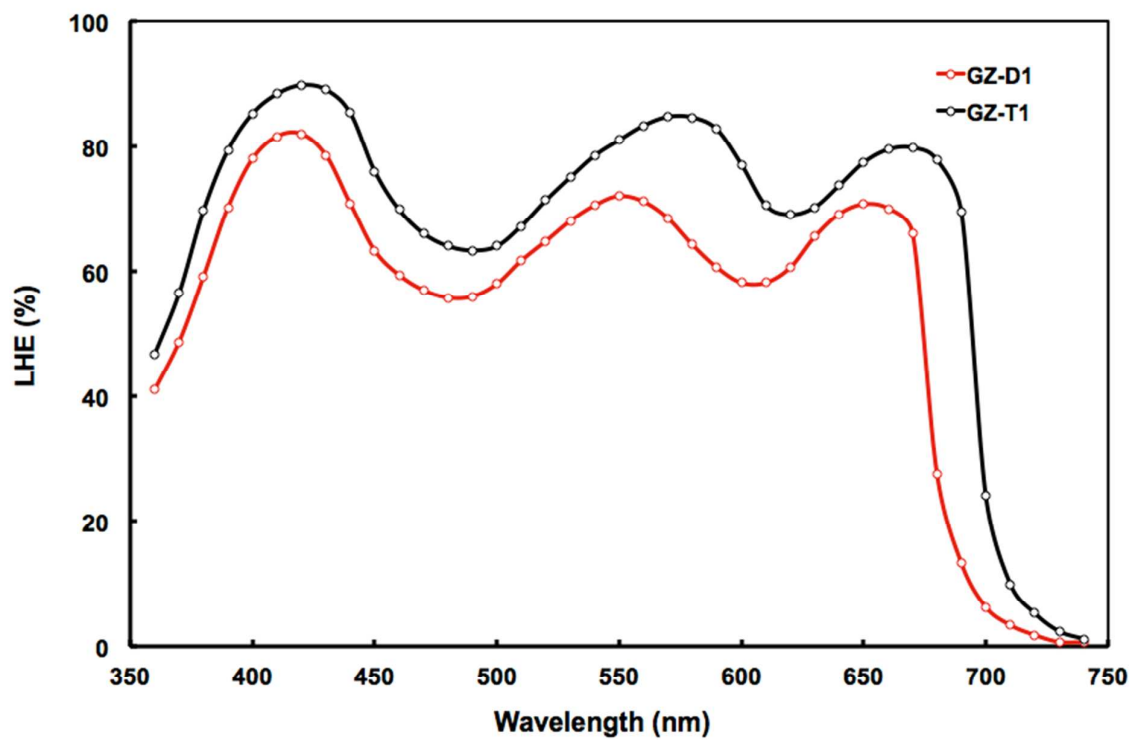
Figure 8: Variation of LHE as a function of wavelength for the DSSCs based on porphyrin dyes **GZ-T1** and **GZ-D1**.
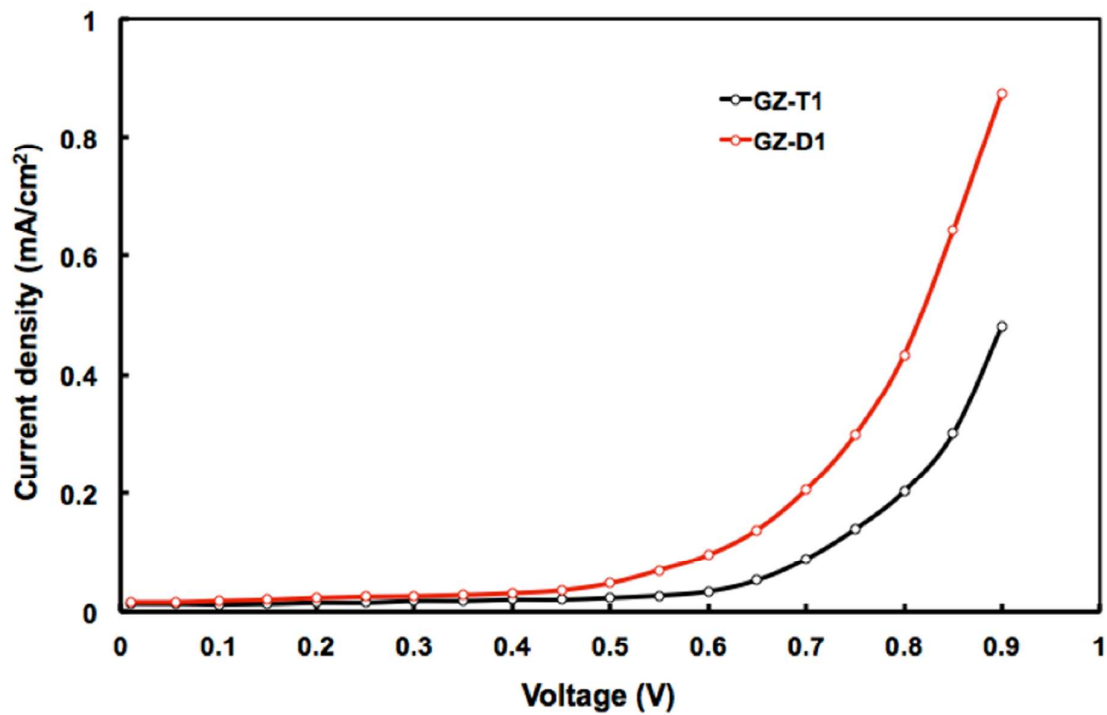
Figure 9: Dark current –voltage characteristics of DSSCs based on **GZ-T1** and **GZ-D1**.
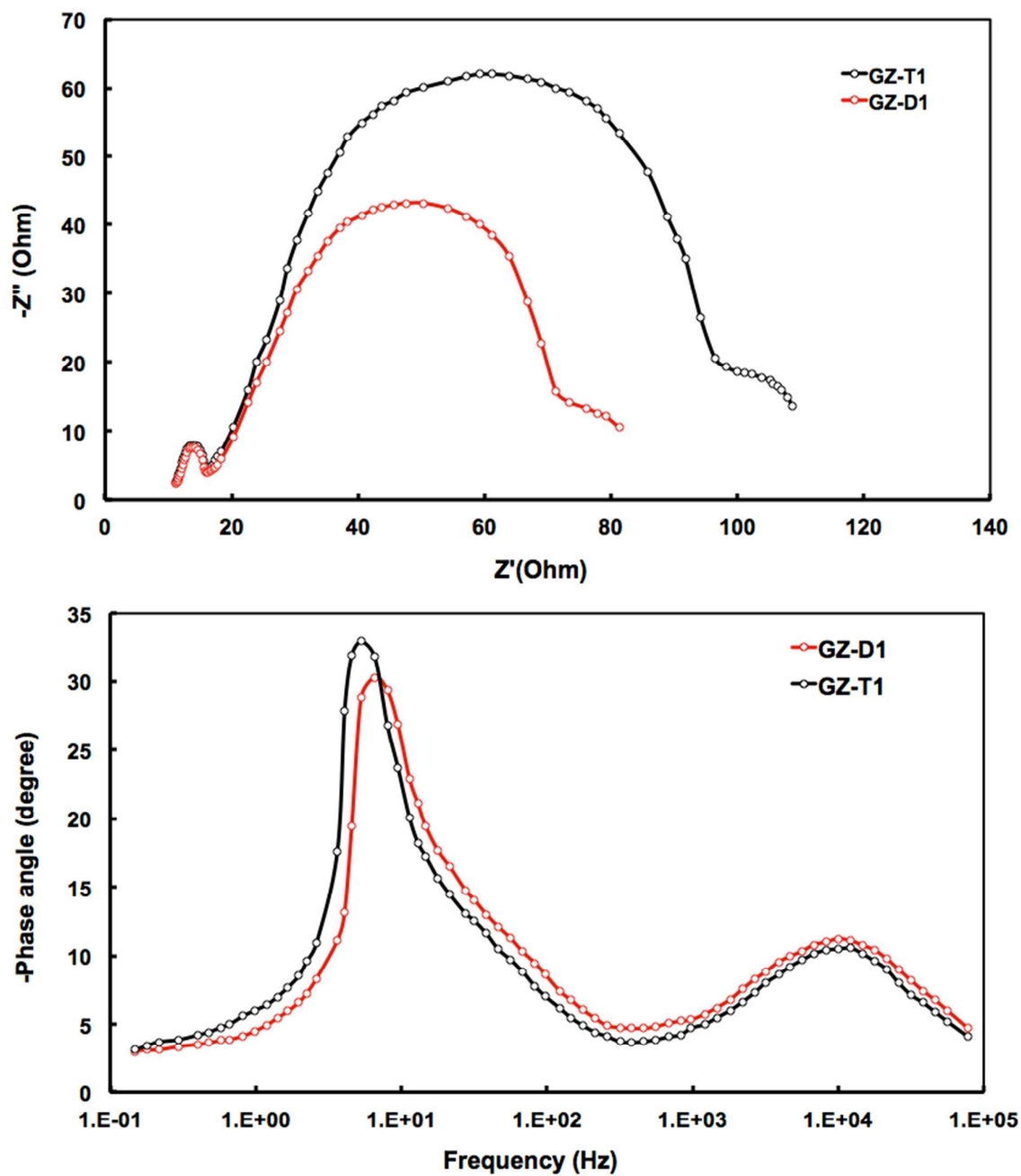
Figure10: (a) Nyquist plots and (b) Bode phase plots of EIS in dark for DSSCs based on **GZ-T1** and **GZ-D1** porphyrin dyes.
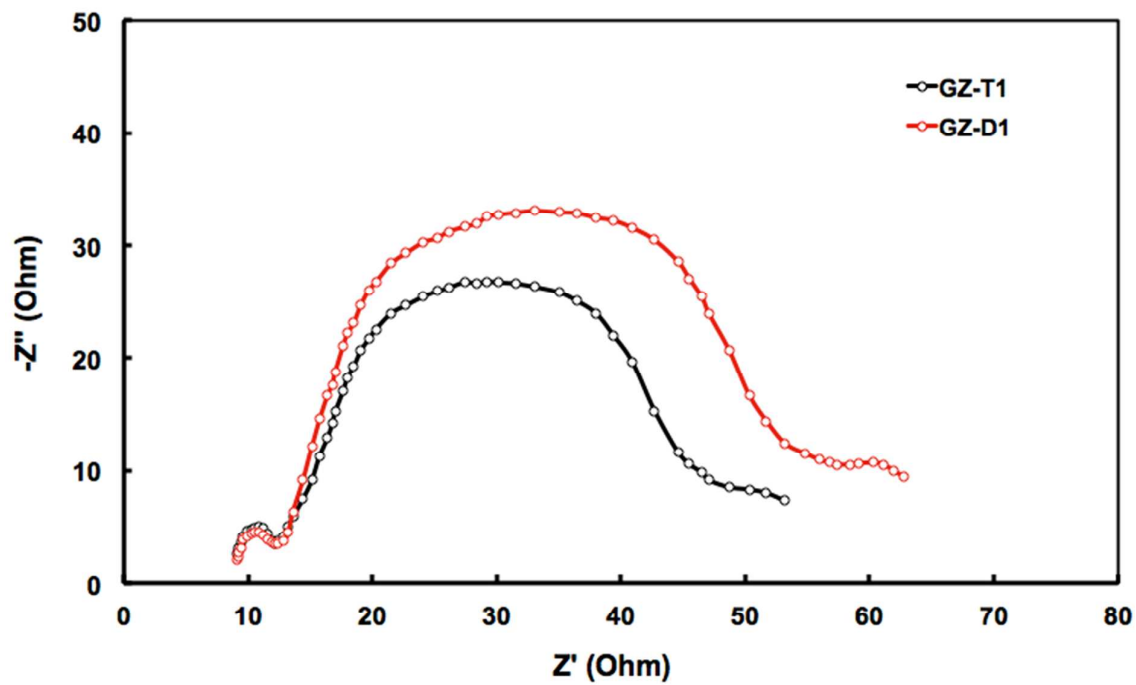
Figure 11: Nyquist plots of EIS under illumination for DSSCs sensitized with **GZ-T1** and **GZ-D1** porphyrin dyes.

References

1 B. O'Regan, M. Grätzel, *Nature*, 1991, **353**, 737-740.

2 (a) L. L. Li, E. W. G. Diau, *Chem. Soc. Rev.*, 2013, **42**, 291-304, (b) A. Hagfeldt, G. Boschloo, L. C. Sun, L. Kloo, H. Pettersson, *Chem. Rev.*, 2010, **110**, 6595-6663.

3 (a) M. K. Nazeeruddin, A. Kay, I. Rodicio, R. Humphry-Baker, E. Mueller, P. Liska, N. Vlachopoulos, M. Grätzel, *J. Am. Chem. Soc.*, 1993, **115**, 6382–6390. (b) P. Péchy, T. Renouard, S. M. Zakeeruddin, R. Humphry-Baker, P. Comte, P. Liska, L. Cevey, E. Costa, V. Shklover, L. Spiccia, G. B. Deacon, C. Bignozzi, M. Grätzel, *J. Am. Chem. Soc.*, 2001, **123**, 1613–1624, (c) M. K. Nazeeruddin, F. De Angelis, S. Fantacci, A. Selloni, G. Viscardi, P. Liska, S. Ito, B. Takeru and M. Grätzel, *J. Am. Chem. Soc.*, 2005, **127**, 16835–16847, (d) F. Gao, Y. Wang, D. Shi, J. Zhang, M. Wang, X. Jing, R. Humphry-Baker, P. Wang, S. M. Zakeeruddin, M. Grätzel, *J. Am. Chem. Soc.*, 2008, **130**, 10720–10728, (e) C. Chen, M. Wang, J. Li, N. Pootrakulchote, L. Alibabaei, C.-H. Ngoc-le, J. Decoppet, J. Tsai, C. Grätzel, C. Wu, S. M. Zakeeruddin, M. Grätzel, *ACS Nano*, 2009, **3**, 3103–3109, (f) L. Han, A. Islam, H. Chen, C. Malapaka, B. Chiranjeevi, S. Zhang, X. Yang, M. Yanagida, *Energy Environ. Sci.*, 2012, 5, 6057–6060

4 (a) A. Mishra, M. K. R. Fischer and P. Bäuerle, *Angew. Chem., Int. Ed.*, 2009, **48**, 2474–2499, (b) Y. Ooyama and Y. Harima, *Eur. J. Org. Chem.*, 2009, **2009**, 2903–2934, (c) W. Zeng, Y. Cao, Y. Bai, Y. Wang, Y. Shi, M. Zhang, F. Wang, C. Pan, P. Wang, *Chem. Mater.*, 2010, **22**, 1915–1925, (d) L.-L. Tan, J.-F. Huang, Y. Shen, L.-M. Xiao, J.-M. Liu, D.-B. Kuang and C.-Y. Su, *J. Mater. Chem. A*, 2014, **2**, 8988–8994

5 (a) W. M. Campbell, A. K. Burrell, D. L. Officer and K. W. Jolley, *Coord. Chem. Rev.*, 2004, **248**, 1363–1379, (b) H. Imahori, T. Umeyama and S. Ito, *Acc. Chem. Res.*, 2009, **42**, 1809–1818, (c) M. V. Martínez-Díaz, G. de la Torre and T. Torres, *Chem. Commun.*, 2010, **46**, 7090–7108, (d) M. J. Griffith, K. Sunahara, P. Wagner, K. Wagner, G. G. Wallace, D. L. Officer, A. Furube, R. Katoh, S. Mori and A. J. Mozer, *Chem. Commun.*, 2012, **48**, 4145–4162, (e) K. Ladomenou, T. N. Kitsopoulos, G. D. Sharma and A. G. Coutsolelos, *RSC Adv.*, 2014, **4**, 21379–21404, (f) T. Higashino, H. Imahori, *Dalton Trans.* 2015, **44**, 448-463, (g) M. Urbani, M. Grätzel, M. K. Nazeeruddin and T. Torres, *Chem. Rev.,* 2014, **114**, 12330–12396, (h) Y. Wang, B. Chen, W. Wu, X. Li, W. Zhu, H. Tian, and Y. Xie, *Angew. Chem. Int. Ed.,* 2014, **53**, 10779–10783

6 (a) T. Dos Santos, A. Morandeira, S. Koops, A. J. Mozer, G. Tsekouras, Y. Dong, P. Wagner, G. Wallace, J. C. Earles, K. C. Gordon, D. Officer, J. R. Durrant, *J. Phys. Chem. C*, 2010, **114**, 3276–3279, (b) M.-E. Ragoussi, G. de la Torre, T. Torres, *Eur. J. Org. Chem.*, 2013, **2013**, 2832–2840.

7 A. Yella, H. W. Lee, H. N. Tsao, C. Yi, A. K. Chandiran, M. K. Nazeeruddin, E. W. G. Diau, C. Y. Yeh, S. M. Zakeeruddin, M. Grätzel, *Science*, 2011, **334**, 629-633.

8 S. Mathew, A. Yella, P. Gao, R. Humphry-Baker, B. F. E. Curchod, N. Ashari-Astani, I. Tavernelli, U. Rothlisberger, M. K. Nazeeruddin, M. Grätzel, *Nat. Chem.*, 2014, **6**, 242-247.

9 (a) C. Lin, Y. Wang, S. Hsu, C. Lo, E. W. Diau, *J. Phys. Chem. C*, 2010, **114**, 687–693, (b) C.-H. Wu, M.-C. Chen, P.-C. Su, H.-H. Kuo, C.-L. Wang, C.-Y. Lu, C.-H. Tsai, C.-C. Wu, C.-Y. Lin, *J. Mater. Chem. A*, 2014, **2**, 991–999.

10 H. Hayashi, A. S. Touchy, Y. Kinjo, K. Kurotobi, Y. Toude, S. Ito, H. Saarenpää, N. V. Tkachenko, H. Lemmetyinen and H. Imahori, *ChemSusChem*, 2013, **6**, 508–517.

11 (a) A. J. Mozer, M. J. Griffith, G. Tsekouras, P. Wagner, G. G. Wallace, S. Mori, K. Sunahara, M. Miyashita, J. C. Earles, K. C. Gordon, L. Du, R. Katoh, A. Furube and D. L. Officer, *J. Am. Chem. Soc.*, 2009, **131**, 15621–15623, (b) K. Sunahara, M. J. Griffith, T.

Uchiyama, P. Wagner, D. L. Officer, G. G. Wallace, A. J. Mozer and S. Mori, *ACS Appl. Mater. Interfaces*, 2013, **5**, 10824–10829.

12 J. K. Park, J. Chen, H. R. Lee, S. W. Park, H. Shinokubo, A. Osuka and D. Kim, *J. Phys. Chem. C*, 2009, **113**, 21956–21963.

13 (a) Y. Liu, H. Lin, J. T. Dy, K. Tamaki, J. Nakazaki, D. Nakayama, S. Uchida, T. Kubo and H. Segawa, *Chem. Commun.*, 2011, **47**, 4010–4012, (b) Y. Liu, H. Lin, J. Li, J. T. Dy, K. Tamaki, J. Nakazaki, D. Nakayama, C. Nishiyama, S. Uchida, T. Kubo and H. Segawa, *Phys. Chem. Chem. Phys.*, 2012, **14**, 16703–16712, (c) T. Hamamura, J. T. Dy, K. Tamaki, J. Nakazaki, S. Uchida, T. Kubo and H. Segawa, *Phys. Chem. Chem. Phys.*, 2014, **16**, 4551–4560, (d) T. Hamamura, J. Nakazaki, S. Uchida, T. Kubo and H. Segawa, *Chem. Lett.*, 2014, **43**, 655–65.

14 (a) H. Zhong, E. Xu, D. Zeng, J. Du, J. Sun, S. Ren, B. Jiang and Q. Fang, *Org. Lett.*, 2008, **10**, 709, (b) J.-W. Kang, D.-S. Lee, H.-D. Park, Y.-S. Park, J.-W. Kim, W.-I. Jeong, K.-M. Yoo, K. Go, S.-H. Kim and J.-J. Kim, *J. Mater. Chem.*, 2007, **17**, 3714; (c) A. P. Kulkarni, C. J. Tonzola, A. Babel and S. A. Jenekhe, *Chem. Mater.*, 2004, **16**, 4556.

15 C. A. M. Afonso, N. M. T. Lourenco, and A. A. Rosatella, *Molecules*, 2006, **11**, 81.

16 (a) S. Ren, D. Zeng, H. Zhong, Y. Wang, S. Qian and Q. J. Fang, *Phys. Chem. B*, 2010, **114**, 10374, (b) H. Zhong, H. Lai and Q. Fang, *J. Phys. Chem. C*, 2011, **115**, 2423.

17 J. Liu, K. Wang, X. Zhnag, C. Li, X. You, *Tetrahedron*, 2013, **69**, 190–200.

18 A. Luechai, J. Gasiorowski, A. Petsom, H. Neugebauer, N. S. Sariciftci and P. Thamyongkit, *J. Mater. Chem.*, 2012, **22**, 23030

19 G. D. Sharma, G. E. Zervaki, P. A. Angaridis, T. N. Kitsopoulos, and A. G. Coutsolelos, *J. Phys. Chem. C*, 2014, **118**, 5968−5977

20 (a) G. Pagona, G. E. Zervaki, A. S. D. Sandanayaka, O. Ito, G. Charalambidis, T. Hasobe, A. G. Coutsolelos, N. Tagmatarchis, *J. Phys. Chem. C*, 2012, **116**, 9439−9449, (b) K. Ladomenou, T. Lazarides, G. Charalambidis, A. G. Coutsolelos, *Inorganic Chemistry*, 2012, **51**, 10548−10556, (c) G. E. Zervaki, M. S. Roy, M. K. Panda, P. A. Angaridis, E. Chrissos, G. D. Sharma and A. G. Coutsolelos, *Inorg. Chem.*, 2013, **52**, 9813−9825, (d) G. E. Zervaki, P. A. Angaridis, E. N. Koukaras, G. D. Sharma and A. G. Coutsolelos, *Inorg. Chem. Front.*, 2014, **1**, 256–270, (e) G. D. Sharma, G. E. Zervaki, K. Ladomenou, E. N. Koukaras, P. P. Angaridis, A. G. Coutsolelos, *J. Porphyrins Phthalocyanines*, 2015, **19**, 175-191, (f) G. E. Zervaki, E. Papastamatakis, P. A. Angaridis, V. Nikolaou, M. Singh, R. Kurchania, T. N. Kitsopoulos, G. D. Sharma and A. G. Coutsolelos, *Eur. J. Inorg. Chem.*, 2014, **2014**, 1020–1033, (g) V. Nikolaou, P. A. Angaridis, G. Charalambidis, G. D. Sharma, A. G. Coutsolelos, *Dalton Trans.*, 2015, **44**, 1734-1747, (h) G. E. Zervaki, A. Nikiforou, V. Nikolaou, G. D. Sharma, A. G. Coutsolelos, *J. Mater. Chem. C*, 2015, DOI: 10.1039/c4tc02902j.

21 J. Lee, Y. Kim, S. K. Kang, I. Choi, J. Yi, *Korean J. Chem. Eng.*, 2006, **23**, 512-515.

22 L. S. W. Kohn, *J. Phys. Rev.*, 1965, **140**, A1133

23 M. Cossi, V. Barone, R. Cammi and J. Tomasi, *Chem Phys Lett*, 1996, **255**, 327-335

24 A. D. Becke, *Phys Rev A*, 1988, **38**, 3098-3100

25 C. T. Lee, W. T. Yang and R. G. Parr, *Phys Rev B*, 1988, **37**, 785-789

26 G. W. T. Gaussian 03; M. J. Frisch, H. B. Schlegel, G. E. Scuseria, M. A. Robb, J. R. Cheeseman, J. A. Montgomery, T. Vreven, K. N. Kudin, J. C. Burant, J. M. Millam, S. S. Lyengar, J. Tomasi, V. Barone, B. Mennucci, M. Cossi, G. Scalmani, N. Rega, G. A. Petersson, H. Nakatsuji, M. Hada, M. Ehara, K. Toyota, R. Fukuda, J. Hasegawa, M. Ishida, T. Nakajima, Y. Honda, O. Kitao, H. Nakai, M. Klene, X. Li, J. E. Knox, H. P. Hratchian, J. B. Cross, V. Bakken, C. Adamo, J. Jaramillo, R. Gomperts, R. E. Stratmann, O. Yazyev, A. J. Austin, R. Cammi, C. Pomelli, J. W. Ochterski, P. Y. Ayala, K.

Morokuma, G. A. Voth, P. Salvador, J. J. Dannenberg, V. G. Zakrzewski, S. Dapprich, A. D. Daniels, M. C. Strain, O. Farkas, D. K. Malick, A. D. Rabuck, K. Raghavachari, J. B. Foresman, J. V. Ortiz, Q. Cui, A. G. Baboul, S. Clifford, J. Cioslowski, B. B. Stefanov, G. Liu, A. Liashenko, P. Piskorz, I. Komaromi, R. L. Martin, D. J. Fox, T. Keith, M. A. Al-Laham, C. Y. Peng, A. Nanayakkara, M. Challacombe, P. M. W. Gill, B. Johnson, W. Chen, M. W. Wong, C. Gonzalez, J. A. Pople, Gaussian 03, rev. D.01, Gaussian, Inc., Wallingford CT, 2004

27 D. A. Z. Zhurko, G. A. ChemCraft 1.6; Plimus: San Diego, CA. Available at http://www.chemcraftprog.com.

28 M. K. Panda, G. D. Sharma, K. R. J. Thomas and A. G. Coutsolelos, *J. Mater. Chem.*, 2012, **22**, 8092–8102.

29 D. W. P. M. Löwik, C. R. Lowe, *Eur. J. Org. Chem.,* 2001, **2001**, 2825-2839.

30 (a) M. B.Steffensen, E. E. Simanek, *Org. Lett.* 2003, **5**, 2359-2361. (b) W. Zhang, E. E. Simanek, *Org. Lett.,*2000, **2**, 843-845

31 T.Lazarides, G.Charalambidis, A.Vuillamy, M.Réglier, E.Klontzas, G.Froudakis, S.Kuhri, D. M. Guldi, and A. G. Coutsolelos, *Inorg. Chem.*, 2011, **50**, 8926–8936.

32 (a) T.Carofiglio, A.Varotto, U.Tonellato, *J. Org. Chem.,* 2004, **69**, 8121-8124. (b) K. Ichihara,Y. Naruta, *Chem. Lett.,* 1995, **24**, 631-632. (c) T. Carofiglio, E. Lubian, I. Menegazzo, G. Saielli, A. Varotto, *J. Org. Chem.,* 2009, **74**, 9034-9043.

33 C.-L. Wang, C.-M. Lan, S.-H. Hong, Y.-F. Wang, T.-Y. Pan, C.-W. Chang, H.-H. Kuo, M.-Y. Kuo, E. W.-G. Diau and C.-Y. Lin, *Energy Environ. Sci.*, 2012, **5**, 6933–6940.

34 R. B. Ambre, G.-F. Chang, M. R. Zanwar, C.-F. Yao, E. W.-G. Diau and C.-H. Hung, *Chem.–Asian J.*, 2013, **8**, 2144.

35 Y. Wang, X. Li, B. Liu, W. Wu, W. Zhu and Y. Xie, *RSC Adv.*, 2013, **3**, 14780–14790.

36 Y. C. Chang, C. L. Wang, T. Y. Pan, S. H. Hong, C. M. Lan, H. H. Kuo, C. F. Lo, H. Y. Hsu, C. Y. Lin, E. W.-G. Diau, *Chem. Commun.*, 2011, **47**, 8910.

37 (a) J. Bisquert, *Phys. Chem. Chem. Phys.*, 2003, **5**, 5360, (b) J. Bisquert, A. Zaban, M. Greenshtein, I. Mora-Sero, *J. Am. Chem. Soc.*, 2004, **126**, 13550. (c) Q. Wang, J. E. Moser, M. Grätzel, *J. Phys. Chem. B*, 2005, **109**, 14945.

38 M. Adachi, M. Sakamoto, J. T. Jiu, Y. Ogata, S. Isoda, *J. Phys. Chem. B*, 2006, **110**, 13872.

39 (a) J. Nissofolk, K. Fredin, A. Hegfeldt, G. Boschloo, *J. Phys.Chem. B*, 2006, **110**, 17715. (b) Q. Wang, Z. Zhang, S.M. Zakeeruddin, M. Grätzel, *J. Phys. Chem. C*, 2008, **112**, 7084.